Julia Marlene Puntigam, BSc

Development of icephobic coatings based on patterned surfaces

MASTER'S THESIS
to achieve the university degree of

Diplom-Ingenieurin (Dipl.-Ing.)

Master's degree programme:

Advanced Materials Science

submitted to
Graz University of Technology

Priv.-Doz. Dr. Anna Maria Coclite

Institute of Solid State Physics

Graz, March 2024

Affidavit

I declare that I have authored this thesis independently, that I have not used other than the declared sources/resources, and that I have explicitly indicated all material which has been quoted either literally or by content from the sources used. The text document uploaded to TUGRAZonline is identical to the present master's thesis.

14.03.2024	
Date	Signature

Abstract

The formation of ice on surfaces can lead to damages to them and hinder machines from working properly in cold conditions. Various techniques are known to delay the formation of ice on top of surfaces, but none are a definite solution to stop the problems caused by it.

Passive anti-icing surfaces have the ability to prohibit ice nucleation and propagation across them, amongst other characteristics. The advantages of passive anti-icing surfaces are, that they do not require any heat or other types of energy to prevent ice from attaching or forming on them.

To create icephobic coatings, surfaces can be coated with polymers. Usually, these coatings have a uniform surface. Inspired by the desert beetle, which can direct the way water flows across its shell by using areas of different wettability, an investigation was started, on how the icephobic abilities of certain coatings change when they are not uniformly applied.

The process of initiated chemical vapour deposition (iCVD) is used to apply polymer coatings onto substrates, creating a pattern. This way, the surface is only partially coated with polymers and areas of the original substrate are still exposed on the surface. The samples with patterned iCVD coatings are then compared to uniformly coated surfaces to investigate how the ice nucleation and frost propagation are influenced by the patterning.

With the patterns, the way water and ice behave on the surface can be influenced and controlled. These innovative ways to create icephobic surfaces can shed further insight into the mechanism and requirements for creating durable and easily reproducible anti-icing coatings.

Kurzfassung

Die Bildung von Eis auf Oberflächen kann zu Schäden auf ihnen führen und dabei Maschinen hindern, unter kalten Bedingungen ordnungsgemäß zu arbeiten. Es gibt verschiedene Techniken, um die Eisbildung auf Oberflächen zu verzögern, aber keine ist eine eindeutige Lösung für die Probleme die Eisbildung verursacht.

Passive Anti-Eis Oberflächen haben unter anderem die Fähigkeit die Eisbildung und die Verbreitung über sich zu verhindern. Die Vorteile von passiven Anti-Eis Oberflächen sind, dass sie keine Hitze oder andere Arten von Energie benötigen, um die Befestigung oder Bildung von Eis auf ihnen zu vermeiden.

Um eisabweisende Oberflächen herzustellen, können Oberflächen mit Polymeren beschichtet werden. Normalerweise haben diese Beschichtung eine einheitliche Oberfläche. Inspiriert von einem in der Wüste lebenden Schwarzkäfer, welcher den Wasserfluss über seinen Panzer durch unterschiedlich benetzbare Gebiete lenken kann, wurde untersucht, wie sich die Eigenschaften von gewissen Beschichtungen ändern, wenn diese nicht gleichmäßig aufgetragen werden.

Mit dem Verfahren der initiierten chemische Gasphasenabscheidung (iCVD) werden Polymerbeschichtungen auf Substraten aufgebracht, in diesem Fall in einem Muster. Auf diese Weise wird die Oberfläche teilweise mit Polymeren beschichtet während Teile des ursprünglichen Substrates auf der Oberfläche unbedeckt bleiben. Die gemusterten iCVD Beschichtungen werden dann mit den einheitlich beschichteten Oberflächen verglichen, um zu untersuchen wie die Eisbildung und Verbreitung durch die Musterung beeinflusst werden.

Mit diesen Mustern kann die Art und Weise wie sich Wasser und Eis auf Oberflächen verhalten gesteuert werden. Diese innovativen Methoden um eisabweisende Oberflächen zu erzeugen können weitere Erkenntnisse über die Mechanismen und Anforderungen für die Entwicklung beständiger und leicht reproduzierbarer eisabweisender Beschichtungen liefern.

Acknowledgements

I would like to extend my thanks to my supervisor Priv.-Doz. Dr. Anna Maria Coclite for her guidance and the passing of her expertise during my master's thesis.

I would also like to thank Gabriel Hernandez Rodriguez for his advice and support with all my experiments.

Additionally, I would like to thank Margherita Aghito for showing me how to use the machines in the lab and answering all the questions I had about them. The iCVD/ALD research group of TUGraz and all the members were great support during my experimental work.

A note of thanks and appreciation to my friends and family who had to tolerate my moods and who had to listen to my troubles with my classes and exams during my studies.

I would like to dedicate this thesis to my grandfather as an acknowledgement for always encouraging me to continue my studies. I would not have been able to graduate without your support.

List of Figures

List of Tables

Acronyms

AFM	.....	Atomic force microscopy
$CuCl_2$	.....	Copper(II) chloride
iCVD	.....	Initiated chemical vapour deposition
mA	.....	Milliampere
mTorr	.....	Millitorr
PFDA	.....	1H, 1H, 2H, 2H, -Perfluorodecyl acrylate
sccm	.....	Standard cubic centimetres per minute
Si	.....	Silicon
SiO_2	.....	Silicon dioxide
T	.....	Temperature
TBPO	.....	tert-butyl peroxide
V4D4	.....	Tetramethyltetravinylcyclotetrasiloxan

Contents

1 Introduction

This thesis aims to assess the effect of patterned surfaces on the anti-icing abilities of surface coatings.

1.1 Motivation

Ice formation on surfaces can lead to damages to them as well as inhibit machines from working properly in cold conditions. Ice formation is problematic for various machines, such as aeroplanes, automobiles, and power cables outside in the cold and wet. [1], [2] Over time, ice can build up and inhibit them from moving and working properly. It can also prohibit sensors and detectors from measuring correctly.

A lot of energy and resources are spent on removing ice from surfaces. A better way would be to prevent ice from forming altogether with the creation of intrinsic anti-icing surfaces. These surfaces have the ability to prevent the formation or adhesion of ice on them. [1], [2] This means, these surfaces can improve efficiency and reduce the costs of machines working in cool environments.

The creation of effective anti-icing coatings is of importance to industries and the improvement of safety.

1.2 Inspiration for patterned surfaces

This thesis is part of a research project: Surfice, a European project on smart surface design for efficient ice protection and control.

The inspiration for the patterned surfaces comes from the desert beetle. This beetle lives in a very arid area where it does not find water very often, so it had to develop an innovative way to survive. Its shell is not smooth but textured, as shown in Figure 1. The shell is hydrophobic with structures on it. The bumps on the shell are hydrophilic. They

collect water out of the air when the humidity is high, which is then funnelled across the hydrophobic parts of the shell to the beetle's mouth. [3]

This natural pattern of a hydrophobic base and hydrophilic structures on top of it is an excellent water collector and diverter. It can influence where the vaporized water in the air condenses and how it moves across the surface. [4], [5]

This pattering approach of biphilic surfaces can be recreated in a lab. Surface coating deposited with initiated chemical vapour deposition can have biphilic properties which could control the ice formation on them. These surfaces are expected to exhibit anti-icing behaviours because of their ability to influence how water behaves on them. Using known hydrophobic monomers, the delay in frost propagation and ice nucleation can be measured. The patterned surfaces are then compared to their non-patterned and uniformly coated counterparts to investigate what effect the patterning has and if the surfaces created with initiated vapour deposition have anti-icing abilities.

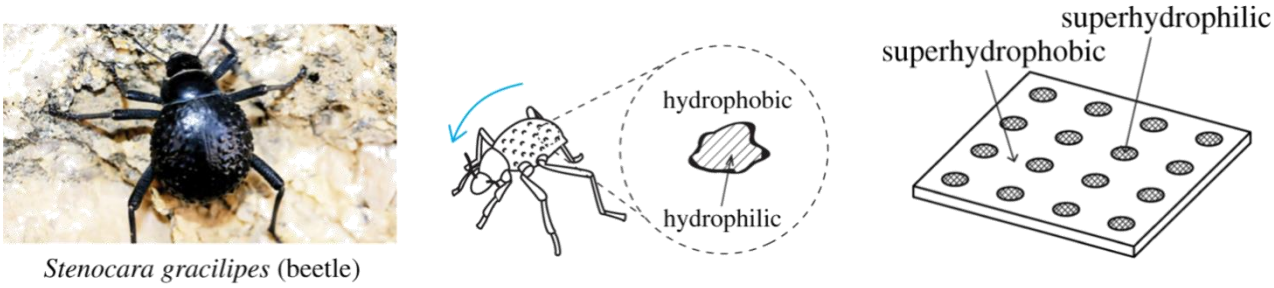

Figure 1: Inspiration for the patterned surfaces comes from the desert beetle. [3]

2 Fundamentals

The initiated chemical vapour process makes it possible to create varying types of functional surfaces. It can be used on almost any type of substrate and the process can be broken down into a few steps. The coatings can be adjusted depending on the desired characteristics they should have. They are easily reproducible, making them interesting for industries that are seeking anti-icing surfaces. [6]

2.1 Initiated chemical vapour deposition process

Initiated chemical vapour deposition, often shorted to iCVD, is the deposition of polymers, without solvents, in which the monomers are led to the substrate in the gas phase. The difference between initiated chemical vapour depositions and regular chemical vapour depositions is, that polymerization can only occur with an initiator starting it. [7]

iCVD reactions necessitate the use of an initiator that is used in combination with the monomer or monomers to create the surface coatings. The initiator is broken down into free radicals by the heating filaments, which lead to radical polymerization of the monomer on the substrate surface. [7]

The iCVD reactor is a vacuum chamber, in which the samples are placed. At least two pumps working in tandem, usually a rotary pump and a turbo molecular pump, are used to create the vacuum inside the reactor. The lid is made of 2.5 cm thick quartz glass for in situ thickness measurements of the coatings with a laser interferometer. A helium–neon laser with a wavelength of 633 nm is used for the thickness measurements during the depositions. [8]

The bottom of the vacuum chamber is a cooling stage which keeps the samples at the desired temperature. The working pressures and the temperature inside the reactor can be set with ribbon heaters and heating pads. A pressure gauge mounted to the reactor gives real-time feedback on the pressure inside the reaction chamber. The flow rates of the precursor or initiator and monomers let into the vacuum chamber can be precisely

set with needle valves. The flow rates of the initiator and the monomers can be set independently of each other. The temperatures of the initiator and monomers can be regulated by heating elements, if necessary. Figure 2 gives an overview of what the iCVD reactor looks like.

The flow rates of the monomers and initiator can be precisely set. The partial pressure of the monomer has to be lower than the saturation pressure of the monomer at that temperature. The relation between the monomer pressure and the saturation pressure influences the speed and the conformality of the depositions. If the ratio is greater than one, the monomers condense on the sample surface which leads to the formation of very rough and ununiform coatings. [7]

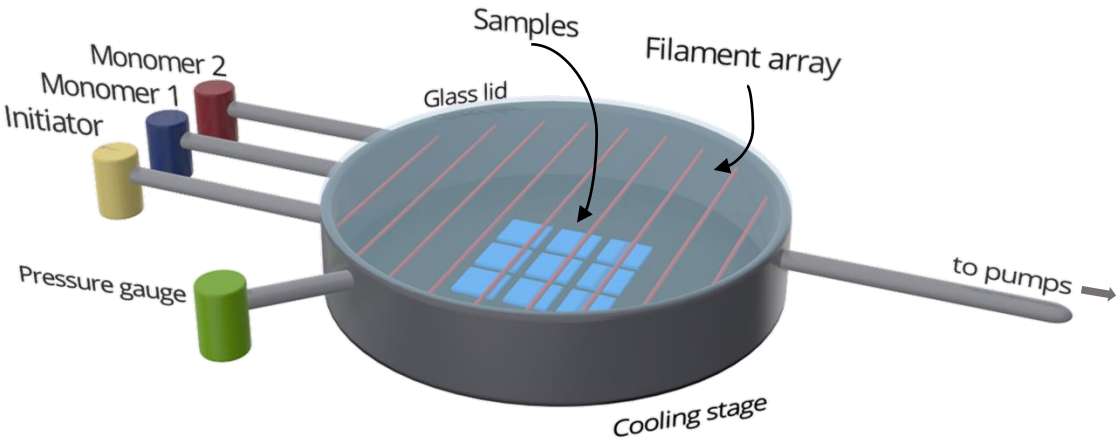

Figure 2: Scheme of an iCVD reactor.

The heated filaments inside the reactor thermally break down the initiator into free radicals once the deposition process is started. The process is depicted in Figure 3. These free radicals then react with the monomers on the surface of the samples, leading to rapid polymerization. No solvents, that could dissolve the exterior of the substrate, are required for iCVD coatings, preserving the surface and its structures beneath it throughout the process. A wide range of coating thicknesses can be achieved with iCVD, ranging from a few nanometres up to several hundred micrometres. [7]

The polymerization is only started once the heated filaments are turned on and have reached the deposition temperature. A critical temperature needs to be reached to break down the initiator. The polymerization also primarily takes place on the cooled substrates, not on the heated reactor walls. This way, the reactor does not get a new surface coating each time an iCVD reaction takes place. Once the filaments are turned

off and begin to cool down, the radical polymerization stops after all the initiator radicals have polymerized. This way the polymerization can be easily controlled.

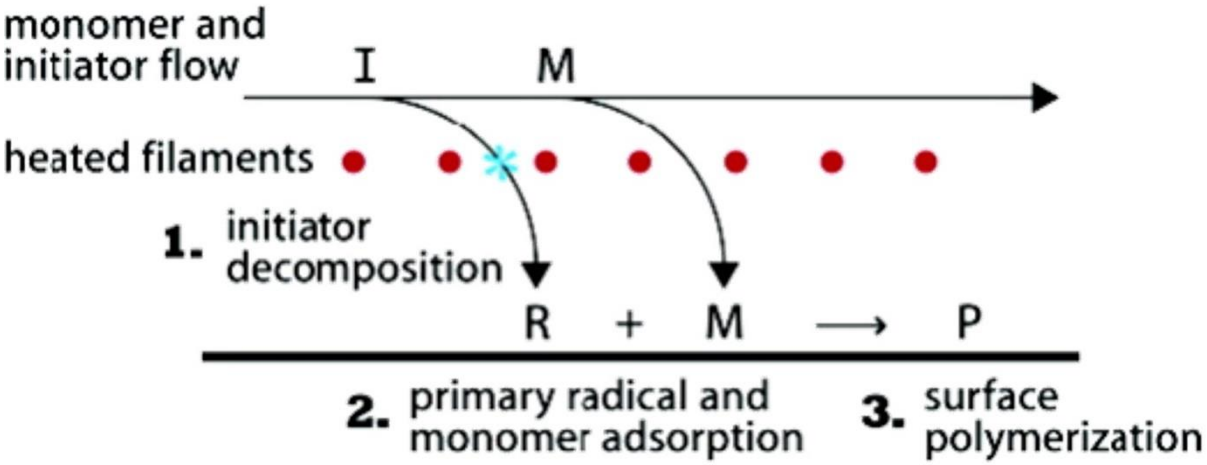

Figure 3: Scheme of radical surface polymerization during iCVD. [7]

With this technique, very smooth, flat and conformal coatings can be achieved. A conformal coating is a uniform coverage of the entire surface and its artifacts. Step edges or structures that might be situated on the surfaces and their sides will be covered by an equally thick coating as the flat areas. No cracks or shadow effects from the structure's form should appear. [7] The coatings are usually durable and long-lasting because they form a tightly cross-linked polymer layer. [1] With iCVD, the surface morphology of the substrate stays intact and is transferred to the surface of the coatings. iCVD coatings can be applied to basically any substrate. It is a dry process that does not need solvents which could destroy the substrate. [9]

2.1.1 Conformal coatings and area selectivity

During the iCVD process usually, the entire surface of an object is covered with chosen monomers. If only certain parts of a surface are to be covered, the deposition on the other parts has to be prohibited. This is similar to how area-selective depositions in photolithography work, where a photoresist layer is cured in selected areas with the help of a photomask. [7]

A similar process is done for iCVD coatings. Areas can be blocked off using inhibitors or masks, which can be seen in Figure 4.

Inhibitors, as their name suggests, prohibit the deposition of the monomers in the areas they are applied to. In the areas covered with inhibitors, no monomer can polymerize and form a coating. [7]

Masks do not prohibit the deposition of monomers, but they shield the surface. Monomers can not reach the areas where a mask is applied, they polymerize on the surface of the mask instead. [7] After the removal of the inhibitor or the mask, the patterned surface is revealed.

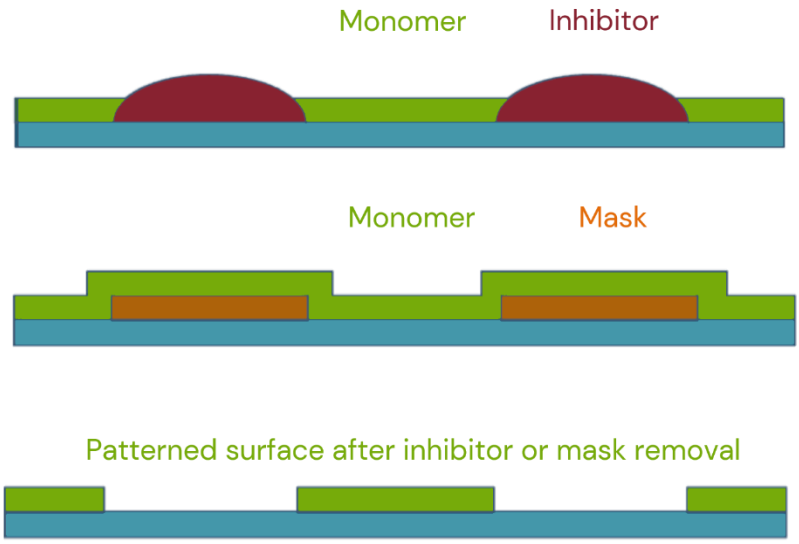

Figure 4: Scheme of patterning with masks and inhibitors during iCVD depositions.

2.2 Icephobicity

The focus of this thesis is the creation of icephobic surfaces. Icephobicity is the term used for surfaces that prevent water from adhering to them, delay the ice nucleation in waterdrops, and have low ice adhesion. [2], [10]

Instead of actively removing ice from surfaces, icephobic surfaces have the built-in ability to hinder ice formation or adhesion. [11]

Countless inquiries into anti-icing surfaces and coatings have already been explored in recent years. A few different processes are known to prevent ice formation on surfaces, which can be categorized into active, passive approaches or mixed. Each method has its challenges and limitations. [2], [12]

Active ways to prevent ice formation, for example, can be mechanical or thermal. Nanostructured surfaces that reduce the water contact angle can reduce the amount of water collecting, or make the drops roll off. [2] Ice that forms on the surfaces can be removed by breaking the ice sheet, scraping it off, or melting it. Passive ways of ice protection can be the creation of water- or icephobic surfaces. The prevention of ice formation on surfaces, along with the delay in frost propagation and reduction in ice adhesion, are important aspects of icephobicity. [11]

The creation of anti-icing surfaces brings a whole new set of problems with it. Water and ice interact differently with surfaces. Water is a liquid and very unstable when placed on surfaces. It can be diverted by superhydrophobic coatings. Ice is a solid that interacts completely differently with surfaces. It attaches to the surfaces with rigid bonds and can withstand shear forces which could damage the surface when it is forcibly removed. [6], [13]

2.2.1 Active anti-icing methods

Active de-icing is the prevention of water accumulation before it can freeze or the removal of the ice after it has already formed.

It can be achieved by mechanically removing the ice from the surface once it has already formed or heating the surface to prohibit the formation of ice completely. [10], [12] This can be achieved in several ways.

The surfaces can be covered in a lubricant that greatly reduces the ice adhesion, causing the ice to detach with minimal force. [10] It needs to be reapplied to the surface as needed; it is not a long-lasting solution, thus counting as an active way of anti-icing. [10]

Resistance heating of surfaces is also another active way to de-ice surfaces, where the surfaces are coated with conductive materials that heat up when an electric charge is applied to them. [14]

Mechanically moving the surface and breaking the ice sheet leads to easier detachment of the ice. Electromechanical systems, a combination of electrical and mechanical methods, can create impulses that remove ice from surfaces. [2]

During the ice removal processes, a lot of forces are enacted on the surfaces, which could lead to damage to them. A way to prevent damage to surfaces during the ice removal process is to prohibit ice formation in the first place. [1], [2]

2.2.2 Passive anti-icing methods

Passive anti-icing methods are very diverse. Different approaches have already been studied.

They can include the creation of superhydrophobic surfaces that hinder water from adhering to the surface and freezing on it. [6] The application of anti-freezing proteins can lower the freezing point of water. [12] Ionic surfaces, which work similarly with anti-freeze proteins, lead to slower ice nucleation and lower ice adhesion on surfaces. [12] Nanostructured anti-frost surfaces limit the spread of frost propagation. [2], [4], [15] If surfaces are hydrophobic enough, waterdrops can jump off of the surface because of the repulsive forces. [16]

Nanostructured surfaces, inspired by the Louts effect, are very hydrophobic. Waterdrops on these surfaces have a very high contact angle because of the Cassie Baxter state. The drops on the surface can easily roll off. These surfaces do delay ice formation to a certain extent. [2], [6]

However, once ice forms on certain nanostructured surfaces, it is very hard to remove. Very fine water droplets can inhabit the air in the spaces between the nanostructures and freeze when the temperature is low enough. The ice can accumulate over time. Once the entire surface is frozen over, the ice is interlocked on those surfaces and difficult to detach. High forces are required to remove the ice from nanostructured surfaces, which can lead to damage to them. [2], [13], [15], [17]

Minimizing ice adhesion to the surface and the delay of frost propagation is an equally important property of icephobic surfaces as the delay of ice formation. Water-repellent surfaces do not have to be icephobic. [13] The difference in adhesion methods between water and ice is quite large. Liquid water can not withstand any sheer force, while ice can. These two things, even though they are the same material in different physical

states, interact completely differently with surfaces. Anti-icing techniques do not have to be water-repellent. [17]

A solution is to create intrinsically icephobic surfaces. Icephobic coatings can slow down ice nucleation, and the formation of ice on the surfaces is delayed. [1] The propagation of frost across the is slow and the adhesion of ice on the surface is low. The creation of surfaces that achieve all three aspects of icephobicity is more difficult than it might seem.

2.2.3 Combined anti-icing methods

Combinations of both approaches have been developed. These include passive anti-icing techniques in combination with active anti-icing strategies, like delaying the ice nucleation in combination with thermal de-icing. [12]

The formation of ice on surfaces can be delayed, but depending on the conditions, it can not be completely prohibited, as it is inevitable. Even very effective icephobic surfaces will get frozen over with enough time at low temperatures. The cooperation of passive and active approaches to anti-icing surfaces seems to promise longer delays in ice formation. [12]

2.2.4 Challenges with anti-icing methods

Every technique of ice prevention brings its challenges with it. There are numerous challenges in creating good anti-icing surfaces. One problem is the creation of long-lasting and durable surface coatings, which provide sufficient ice protection. [1] A better approach is to generate a surface that has the built-in ability to prevent ice formation.

Active ice prevention mechanisms require energy and monitoring and must be reapplied in certain circumstances like anti-icing lubricants. Many passive ways do delay the ice formation, but do not prohibit it completely, meaning the surfaces will be covered in a sheet of ice after enough time has passed. [10], [12]

The research into anti-icing is driven by the need to ensure machines can function properly and guarantee safety when faced with cold and wet conditions. Until now

there has not been found one solution to prevent ice and frost from forming on surfaces. It can only be delayed to a certain extent. [2], [11], [12]

Because of the different adhesion mechanisms of water and ice, there does not have to be a clear correlation between hydrophobicity and icephobicity. Hydrophilic anti-icing coatings using anti-freeze proteins have been achieved. [13]

2.3 Anti-icing surface coatings with iCVD

Anti-icing coatings have already been achieved with iCVD, most often based on the development of superhydrophobic coatings.

Superhydrophobic coatings have been created with iCVD by Mohammadian et al., which lead to a delay in frost propagation due to the de-wetting of waterdrops. Substrates can be covered in polymers and be made so hydrophobic, that waterdrops jump or sweep off of them on their own. [4]

These superhydrophobic coatings bring their own set of problems with them. For example, water vapour can attach between the structures, freeze, and lead to faster ice nucleation and frost propagation, under the right conditions. [6], [13], [15]

A novel way to approach the creation of icephobic iCVD coatings is the application in a gradient, which has been studied by Huang et al., using two polymers. One polymer is applied to the substrate before a mixture of two polymers is deposited. The cross-section of these gradients shows a gradual change from polymer one to a mixture of both. The thickness of the different sections can tune the characteristics of the coating. [18], [19]

A combination of the monomers V4D4 and PFDA has been investigated by Hernández Rodríguez et al., creating gradient copolymers with high surface roughness. The coatings achieved with those two monomers were highly cross-linked and showed promising icephobic abilities. The ice adhesion is greatly reduced when compared to uncoated silicon substrates. The force required to remove ice that has formed on the surface is low. The drop freezing is greatly delayed, with drops staying liquid on surfaces cooled down to -20°C for hours. The condensation and the frost propagation across the gradient polymer surfaces are delayed. [19]

The icephobicity of the gradient copolymers can be tuned by changing the thickness of different sections of the coatings, mainly the PFDA top layer. The structure of the PFDA top coating depends on the thickness. Close to the copolymer, the PFDA in the

coating is arranged in-plane. The direction changes with increasing distance from in-plane to out-of-plane before switching to a random arrangement. All investigated coatings had three sections with different orientations of the PFDA, with the thickest coating having the largest random-orientation layer. [19]

3 Substrate and sample preparation

The iCVD depositions were all done under the same conditions to achieve the same quality of surface coatings with equal thickness and structure.

3.1 Monomers

Two monomers and one initiator were used to create the sample coatings. The initiator used was tert-butyl peroxide or TBPO. It is thermally broken down by the heated filaments. The initiator radicals react with the monomers in the gas phase, leading to monomer absorption and surface polymerization on the substrate surface. [7]

The monomers used to create the icephobic surfaces are Tetramethyltetravinylcyclotetrasiloxan or V4D4 and PFDA, also known as 1H, 1H, 2H, 2H, -Perfluorodecyl acrylate. Research into superhydrophobic coatings and even icephobic coatings using these two monomers has already been conducted. [4], [19]

V4D4 is used as a base coating to make it possible to deposit PFDA on a silicon substrate. PFDA alone has a low adhesion to silicon. The combination of these two monomers as a stacked polymer makes it possible to create durable and robust surface coatings on various types of substrates. [20]

3.2 Pattern search

To create surfaces with distinctly different areas, the samples needed to be patterned. An inhibitor and a mask were tested. The inhibitor was $CuCl_2$, which is a metal salt in an aqueous solution. [21] It was applied with an aerosol dispenser to achieve a completely random pattern.

The mask was Kapton tape, which was laser cut. This mask is a very inexpensive but also simple and easily reproducible technique to perform area-selective iCVD. Both, the initiator and the mask were tested before one was picked to create the samples for the icing and frost propagation experiments.

3.2.1 $CuCl_2$ inhibitor

$CuCl_2$ is a metal salt. [21] The $CuCl_2$ was dissolved in distilled water in different molarities and then applied to the samples with an aerosol dispenser. The patterning worked with different strengths of the aqueous solutions; the dot sizes varied with the molarities as well as the height and technique they were applied with. Higher molarities of the $CuCl_2$ solution led to bigger holes on the surface of the top coating. The drop sizes were the same for all molarities, but after the water evaporated, the amount of $CuCl_2$ left behind was higher for solutions with larger molarities. The polymer could still deposit on the areas where the $CuCl_2$ solution evaporated and no $CuCl_2$ salt was left behind, to some extent, but not in the same thickness as in areas where the $CuCl_2$ solution was not applied. The height, from which the $CuCl_2$ was applied to the surface with an aerosol dispenser, also changed the sizes of the drops slightly. To ensure all the samples were patterned the same the solutions were applied from a distance of 30 cm.

Picture (a) of Figure 5 shows a hydrophobic surface with the $CuCl_2$ inhibitor. The solution formed small drops in a random pattern on the V4D4 surface. Picture (b) shows a sample that had a V4D4 base coat that was patterned with $CuCl_2$ after the deposition of PFDA on top and the removal of the inhibitor. The pattern is visible to the naked eye and completely random with differently sized circles.

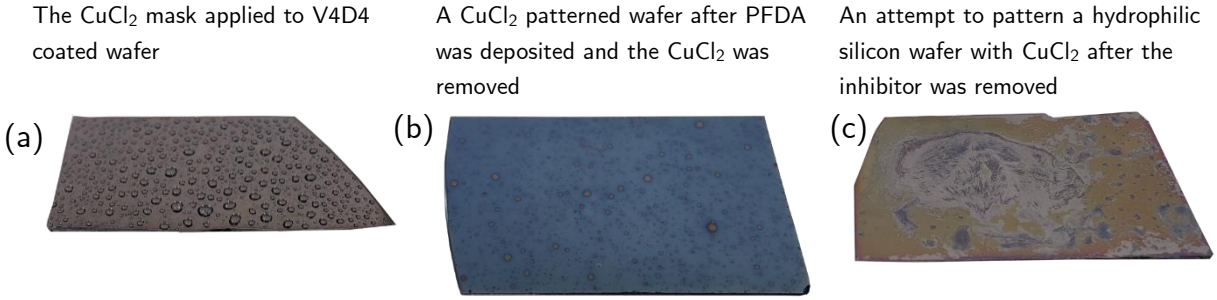

Figure 5: $CuCl_2$ pattering approach and results.

When applying the $CuCl_2$ solution to hydrophilic surfaces, like plain silicon, the drops started to form one big blot and no fine pattern. Picture (c) shows a plain silicon wafer that was patterned with $CuCl_2$ after an iCVD deposition. No pattern was distinguishable. Because the $CuCl_2$ only worked on hydrophobic surfaces, the decision was made not to use this inhibitor to produce samples for the experiments.

3.2.2 Kapton tape mask

In tandem with the inhibitor, a mask was investigated for area-selective iCVD. Kapton tape is inexpensive and masks made of it are easily reproducible. Kapton tape is safe to use inside vacuum chambers because of its low outgassing properties and structural stability across a wide range of temperatures. It is easy to handle and is widely available in different sizes and thicknesses. [22]

Different ways of masking the samples with Kapton tape were explored. The Kapton tape that was used had a thickness of 50 µm. Initially, the Kapton tape was cut with scissors, which led to big and not very reducible patterns. A faster and more precise method to cut the tape was with the laser cutter. For this method, the Kapton tape is placed on a metal cutting board, which is then placed inside the laser cutter. A metal board is needed as a base to stabilize the Kapton tape while it is cut, and to be able to peel the tape off the cutting board without damaging it.

Different patterns were considered. If the pattern was too big and the distances between the holes were too small, the stability of the Kapton tape was lost. It was difficult to handle and apply it to the samples. Large holes with only small tape strips between them led to the Kapton tape ripping easily.

A starburst pattern was tried, which worked, but the spacing between the masked and unmasked areas was too big for the planned measurements. The waterdrops used during the measurements were too small to reach both areas that were masked and unmasked during the deposition. Increasing the number of spikes of the starburst pattern reduced the stability of the Kapton tape, so this pattern could not be used for the desired experiments.

The laser cutter was limited to cut lines with a minimum thickness of around 0.1 mm. It was not possible to cut smaller holes in a pattern into the Kapton tape.

3.2.3 Pattern selection

In the end, the decision was made to just use Katon tape as a mask for the area-selective iCVD coatings. Three different diameters of circular holes were cut into the Kapton tape. For the smallest pattern, 0.1 mm holes were cut into the tape. For the larger pattern, 0.5 mm and 1 mm holes were laser cut into the Kapton tape. The spacing between the edges of the holes was 0.5 mm. This means that there was a 0.5 mm thick Kapton tape framework between the holes. If the distance between the cuts was smaller, the tape tended to rip when it was removed from the metal cutting board.

Circular holes were cut into the tape with a laser cutter so that the dots themselves were isotropic. Shapes with sharp edges like rectangles or hexagons could influence how the water or ice on the surface behaves. Patterned lines on the surface could lead to directional-dependent icing behaviour. The circles should have fewer sharp edges that could enhance the water condensation and ice nucleation during the experiments.

Picture (a) in Figure 6 shows what the Kapton tape mask looked like before the deposition of the iCVD coating. Pictures (b), (c) and (d) show how the patterned surfaces with the differently sized dots looked like after the mask was removed and the wafers were cleaned in a sonic isopropanol bath.

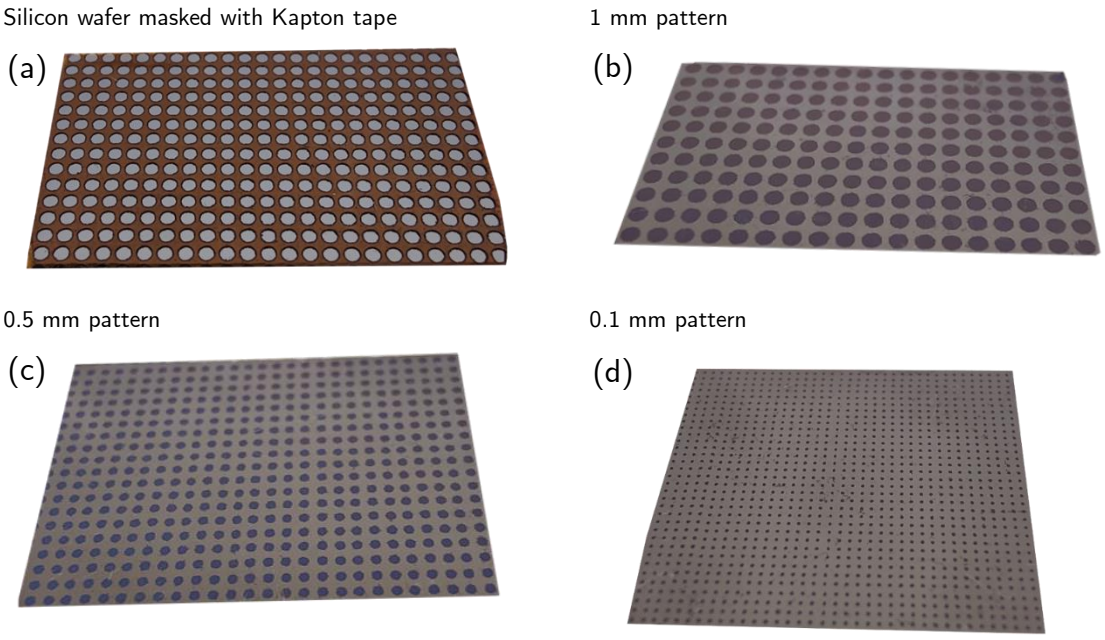

Figure 6: Samples patterned with Kapton tape.

3.3 Substrate preparation

The substrates for the iCVD coatings were one-millimetre-thick silicon wafers cut into roughly two-by-two-centimetre pieces. The sample size was chosen because of the maximum observable area during the icing and frost propagation experiments. Bigger samples would not have fit into some setups of the experiments and the surface area of the wafer would have been too big to observe and monitor during the experiments.

The silicon wafers were cut with a diamond cutting pen and handled with gloves during all the following steps. After the silicon wafer was cut, the pieces were cleaned for ten minutes in a sonic isopropanol bath. Then they were blow-dried with CO_2 gas to prohibit any isopropanol residue.

3.4 iCVD setup

The samples were placed in the reactor before the glass lid was closed and the air in the vacuum chamber was pumped away. It took a few hours until a low enough vacuum was reached again, usually, the samples were left in the reaction chamber overnight. The leak rate of the chamber needed to be low and very stable to precisely measure the flow rates of the monomers.

Conditions and parameters for the iCVD reaction needed to be set before the reaction was started. The iCVD settings used for the depositions are listed in Table 1. All depositions were done with the same settings to ensure they were identical and performed under the same conditions.

Initially, the base pressure in the vacuum chamber was measured. This measurement was subtracted from all flow rates to give the exact amount of the monomer let into the reaction chamber. Then the leak rate was measured. This is the volume of gas seeping into the reactor because of leaks. The longer the reactor is left closed, the lower and more stable the base pressure and the leak rate tend to get until the lower limit of the vacuum pumps is reached.

The parameters the reactor was set to are listed in Table 1. The top of the reactor was heated with a heating pad set to 60°C while the cooling stage at the bottom of the reactor was set to 40°C. This way, the temperature inside the reactor was 60°C and

only the bottom of the samples was cooled to 40°C. The cooler samples, in comparison to the hotter reactor, made the sample surfaces favourable for the radical polymerization of the monomers instead of the reactor walls.

Then the flow rates of the initiator and monomers were measured. The inlet line for the initiator was opened. The pressure in the vacuum chamber perceptively spiked until a new base pressure with the open inlet line was reached. Then the flow rate of the initiator could be measured. The flow rate was set to 1 sccm by adjusting the needle valve of the inlet line. The flow rate was measured at least three to five times to confirm that it was stable. Then the inlet line was closed again without adjusting the needle valve. This process of opening the inlet valves, letting the pressure in the reaction chamber adjust, and measuring and setting the flow rates before turning off the inlet lines was repeated for the monomers.

Table 1: iCVD reactor settings and conditions

Base pressure	<12 mTorr
Leak rate	<0.01 mTorr
Deposition pressure	500 mTorr
Deposition temperature	60°C
TBPO flow rate	~1 sccm
V4D4 flow rate	~0.2 sccm
PFDA flow rate	~0.05 sccm
Reactor temperature	60°C
Cooling stage temperature	40°C
TBPO temperature	Room T
V4D4 temperature	~100°C
PFDA temperature	~90°C
Filament power	1.15 mA
Filament temperature	~200°C

3.5 iCVD deposition process

In contrast to CVD, the iCVD process only works when an initiator is used. In conventional CVD, the monomers react with each other in the gas phase and form a polymer film on the sample surface. During the iCVD depositions, the reactions are more controlled and can be managed by the initiator. Unless the initiator molecules are let into the reaction chamber, no polymerization occurs. The initiator can be thermally activated or by UV light. [7]

Before a deposition is started, all the reactor settings need to be set. The pressure and the temperature in the reactor and of the monomers need to be correct.

To achieve a coating with a monomer, the initiator line is opened first. Once the pressure inside the reactor stabilizes, the line for the monomer is opened. Lastly, the heated filaments are turned on. These thermally break down the initiator into free radicals, which lead to surface polymerization of the monomers on top of the samples.

To achieve the gradient copolymers, first, a layer of V4D4 is deposited. Once the desired thickness of the V4D4 coating is reached, the inlet line for the PFDA is opened and a copolymer of V4D4 and PFDA is applied on top of the base layer. After the copolymer reaches the desired thickness, the V4D4 inlet line is turned off and only a PFDA polymer is deposited on top of the copolymer.

To stop the deposition process, the monomer flows into the reaction chamber are stopped to allow the initiator to polymerize all the monomers still in the reaction chamber. After a waiting period of about a minute, the initiator flow into the reaction chamber is stopped. This allows all the initiator radicals in the vacuum chamber to cap all the dangling bonds on the polymer surface. After another short waiting period, the heated filaments are turned off and the reaction chamber is vacuumed again. The depositions have stopped.

The thicknesses of the coatings are measured with an interferometer during the depositions, making it possible to gauge their thickness during the depositions and choose the right moment to open and close the inlet lines of the monomers.

This way, a mixture between a gradient and a stacked copolymer is achieved as depicted in Figure 7. A base layer of V4D4 guarantees the adhesion of the copolymer to the substrate. PFDA has poor adhesion to silicon surfaces. The copolymer in the middle helps the PFDA adhere to the V4D4 and the pure PFDA top layer is responsible for the coating characteristics on the surface. [20]

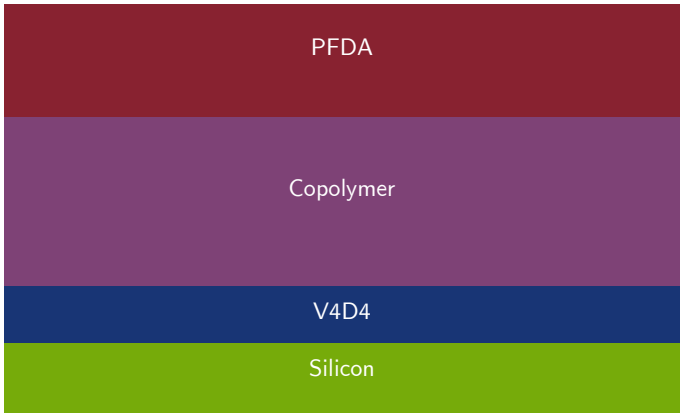

Figure 7: Structure of the gradient copolymer.

3.6 Types of surface patterning

Two different hydrophobic monomers, V4D4 and PFDA, are used to create the patterned surfaces on silicon substrates. The difference between them is depicted in Figure 8.

Superhydrophobic coatings using these two monomers have been achieved and icephobic copolymer coatings using these monomers are researched at TUGraz. [6], [19]

The monomers were deposited on the silicon wafers in two different ways. For method one, the entire surface was covered with a uniform coating of V4D4 and PFDA was applied in a pattern on top of it. The entire surface is hydrophobic, but the coating is patterned, not homogeneous.

For the second method, the plain silicon wafers were masked and then a gradient copolymer of those two monomers was deposited.

The copolymer spots on a base of plain silicon form a biphilic surface, which resembles the natural patterning approach of the shell of the desert beetle.

The effects of a patterned hydrophobic surface versus a patterned biphilic surface on the ice formation and the frost propagation were observed during the ice nucleation and frost propagation experiments.

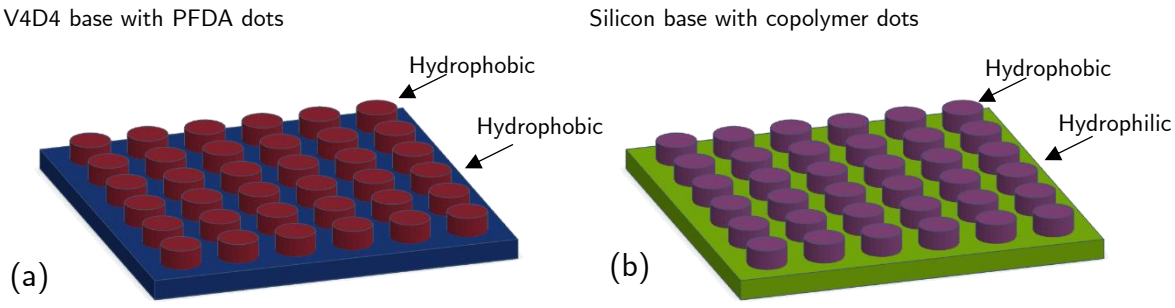

Figure 8: The two different types of patterned surfaces.

3.6.1 Coatings and patterning process

Two different types of surface coatings using the two monomers, V4D4 and PFDA, were created using two different methods. One coating is patterned hydrophobic, and the other is patterned biphilic. The patterning process can be seen in Figure 9.

For method one, a 50 nm thick coating of V4D4 was deposited with iCVD. Then the samples are removed from the reactor and the Kapton tape with the three different patterns is applied to the base coating. The samples were put back into the iCVD reactor and a 100 nm thick coating of PFDA was applied on top.

Then the samples are taken out of the reactor again and the Kapton tape is carefully peeled off. After the masks are removed, the patterned surfaces are revealed. The wafers are cleaned in an isopropanol bath to remove the glue residue.

In total, the coating thickness for the patterned hydrophobic surface of method one is 150 nm.

For method 2 the laser-cut Kapton tape with the three different-sized holes was directly applied onto the cleaned silicon surface and the samples were placed in the iCVD reactor. Then a 50 nm thick base coating of V4D4 was applied before the line for PFDA was opened to deposit a 150 nm thick copolymer. The V4D4 was turned off and a 100 nm thick coating of only PFDA was deposited on top. This copolymer was done with the same setting and of the same thickness as other copolymer coatings that are currently researched at TUGraz. [19]

After the deposition is finished, the samples are taken out of the reactor, the Kapton tape is peeled off and they are cleaned in an isopropanol bath.

In total, the coating thickness for the patterned biphilic samples of method two is 300 nm.

V4D4 is needed as a base layer for PFDA on silicon substrates. PFDA alone does polymerize on Si, but the coatings are very unstable and easily detach from the substrate surface. [20]

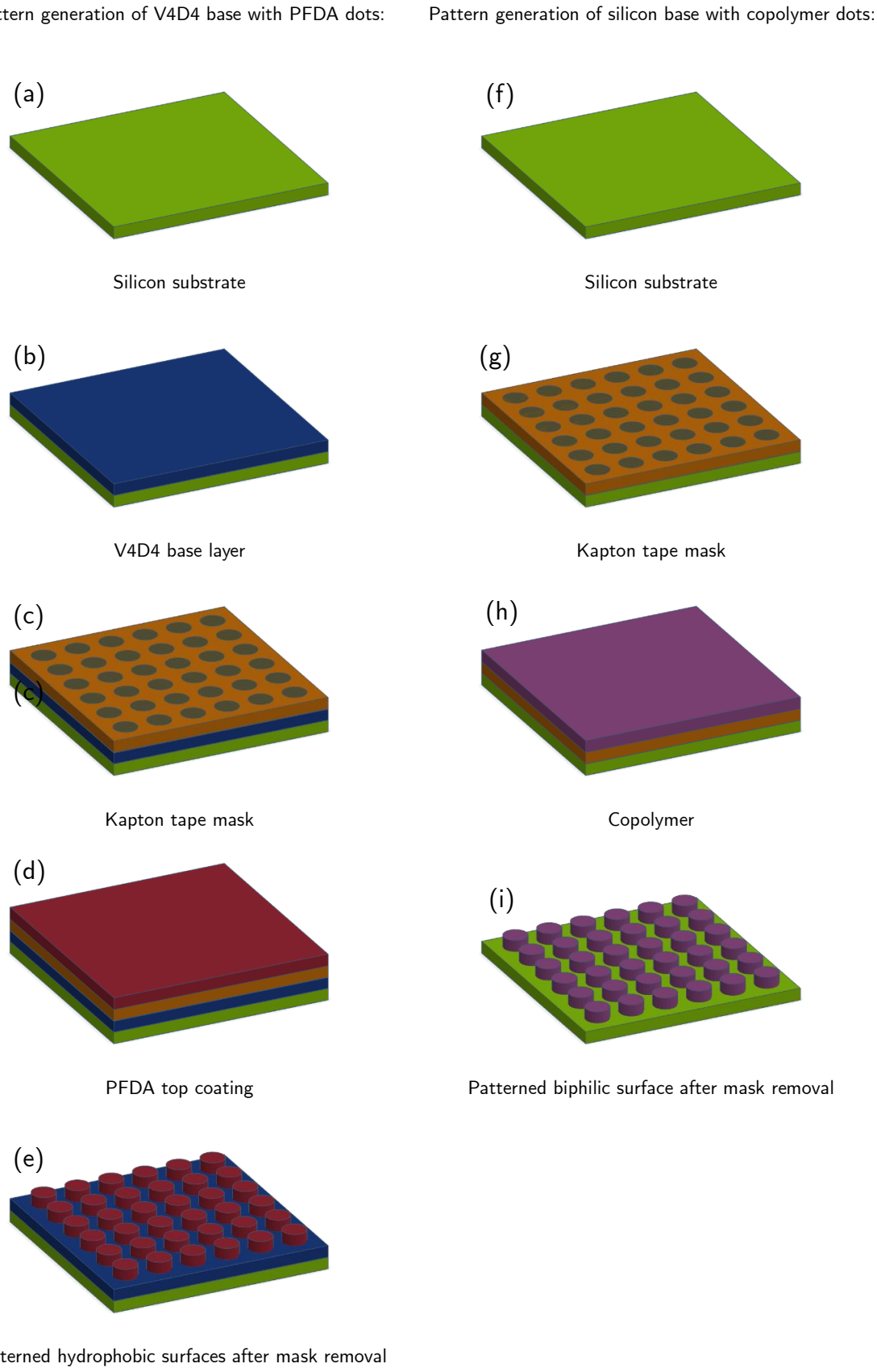

Figure 9: Two different modes of pattern generation.

3.6.2 Disadvantages of the patterning techniques

To create the patterned surface, the Kapton tape needs to be applied directly to the sample surface. This means the sample surfaces will be contaminated by the glue from the tape and other debris. During the cutting of the Kapton tape, the holes are burned into it by a laser. This means a lot of burnt pieces and carbon particles are left behind. After the Kapton tape is cut, the burned pieces are blown off with air, before the top of the tape is cleaned multiple times with isopropanol. This is repeated until no more black particles come off of the laser-cut tape. The underside of the tape can not be cleaned, because the adhesive needs to stay intact. This means that if any burnt pieces manage to stick to the underside of the Kapton tape, they will come in contact with the sample surface. If there are too many of these burnt pieces left behind, they will inhibit the functionality of the mask and lead to the monomers leaking under it during the depositions. The adhesive material touching the sample surface can not be avoided.

For the hydrophobic pattern, the samples need to be taken out of the reactor after the base coating of the V4D4 was completed, to put the mask on the sample surfaces. This means the surfaces are exposed to the ambient environment, while the mask is applied.

The mask is directly applied to the silicon samples once they are cleaned to create the biphilic samples. Then the surfaces of the masked samples are blown off with CO_2 to remove any surface contaminations and burnt particles before they are placed in the reactor.

Once the mask is applied to the samples, they can not be cleaned anymore, this would inhibit the adhesive from working properly. Quite a lot of pressure is needed to apply the tape to the silicon surface to ensure the mask is prohibiting the monomers from reaching the sample surface. This was done with a silicone rolling pin and a plastic scraper to make sure every part of the mask was stuck on the sample surface. The mask application is a quite rough physical process that can lead to scratches or other damage to the sample surface. It is not a clean process.

The samples can even break during the mask application process, because of the forces required to press the mask to the sample surfaces. If the mask is just laid across the surface, it will not adequately shield it during the depositions. The monomers leaking under the Kapton tape destroy the carefully created patterns.

When the mask is removed from the samples after the depositions, the uniform coating of the polymers is broken. This means there are jagged edges around the patterned dots, which can be seen in the atomic force microscopy images. High surface artifacts are detected on the edges of the patterned dots with atomic force microscopy. This is a part of the working mechanism of the mask and can not be avoided. The breaking points of the polymer are usually around the edges of the patterned dots, which is the weak point of the coating.

Once the mask is removed, the samples need to be cleaned in an isopropanol bath to remove the glue residue that is left behind. This step is important and needs to be done before any surface characterization tests can be performed.

4 Results

Different techniques were utilized to characterize the patterned sample surfaces and their unpatterned, uniformly coated counterparts. The better the surfaces are understood, the easier is it to conclude the experimental data.

4.1 Surface morphology

Optical microscopy was performed on the samples after they were taken out of the reactor and cleaned in a sonic isopropanol bath for ten minutes. The microscopy pictures were taken at room temperature in the ambient air.

Figure 10 shows optical microscopy pictures of a sample that was patterned with a $CuCl_2$ mask. A hydrophobic coating of V4D4 was applied to the samples before they were patterned with the $CuCl_2$ inhibitor and a top coat of PFDA was deposited. Then the inhibitor was removed, and the samples were cleaned. The circles visible on the surface are the areas where the top coating was not deposited, these are holes in the top coating. The bluish or purple-coloured areas in Figure 10 are areas where the top coating of PFDA was deposited. The red or orange circles are the holes in the top coating, here the V4D4 base layer is still visible. The pattern is completely random with differently sized dots and spacing between them.

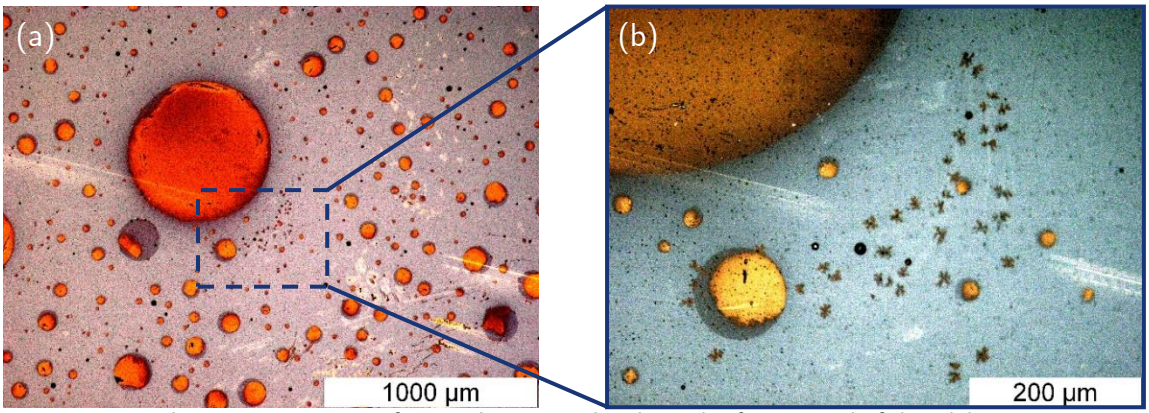

Figure 10: Optical microscopy picture of a sample patterned with $CuCl_2$ after removal of the inhibitor.

Figure 11 shows optical microscopy pictures of wafers after the deposition and removal of the Kapton tape mask. The lighter areas are the plain silicon base and the dark spots are the areas where the copolymer was deposited.

Picture (a) is a wafer that was patterned with Kapton tape that had 0.1 mm holes cut into it. Picture (b) in the middle shows a wafer that was patterned with 0.5 mm holes and picture (c) on the right shows the biggest dot size of 1 mm.

The Kapton tape is a very simple technique, but the result is good. The dots are all in circular shapes and they are roughly the desired diameters. During the application of the Kapton tape, quite a lot of force is needed to press it down on the sample to prevent the monomers from bleeding under it during the iCVD process. In some areas, some of the monomer radicals still managed to seep under the mask, causing the dots not to be perfect circles. This is especially true for the smallest pattern with 0.1 mm holes. Overall, the mask worked with minor problems, and the patterned surfaces were used for the icing tests.

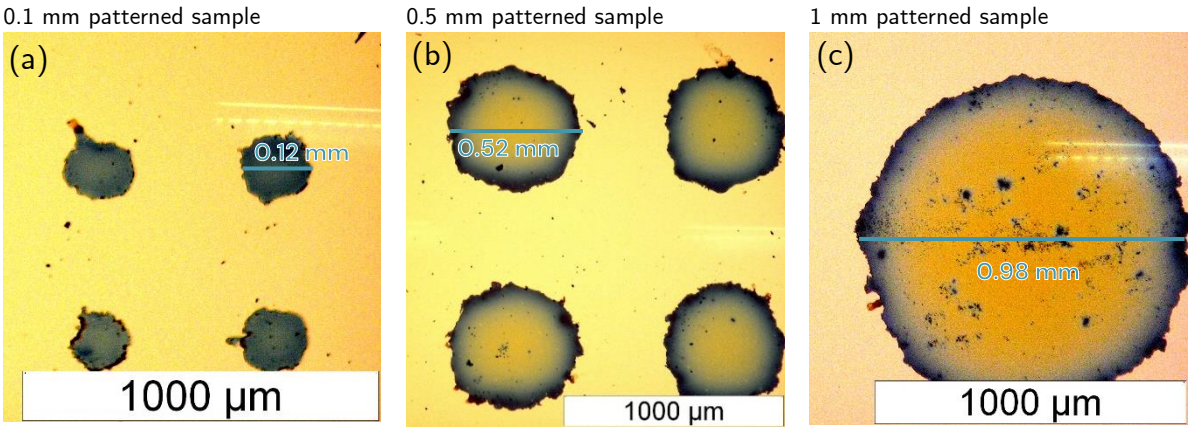

Figure 11: Optical microscopy pictures of silicon wafers patterned with Kapton tape after the Kapton tape was removed.

4.1.1 Surface coverage by the patterned dots

Because of the different-sized dots, the surface coverage of the patterned top layer of the samples varies. The surface coverage depending on the dot sizes can be seen in Table 2. The surface coverage was calculated from optical microscopy pictures of the different patterns with the program ImageJ.

The surface coverage is especially of significance for the biphilic pattern, where the percentage of the hydrophobic dots increases with the size of the dots. For the smallest dots, less than 15% of the surface is hydrophobic. Even though only a small part of the base layer is covered, the samples seemed to behave similarly to the ones with a larger surface coverage during the icing and frost propagation experiments.

Table 2: Surface coverage of the different patterns

Dot size	Spacing between dots	Surface coverage
1 mm	0.5 mm	~13%
0.5 mm	0.5 mm	~36%
0.1 mm	0.5 mm	~50%

4.1.2 Surface defects

Surface defects in a few of the coatings could be seen using optical microscopy.

Especially the thin coatings tended to show surface imperfections. These were snowflake-shaped holes in the surface coating, dispersed randomly across the whole sample surface. The applied V4D4 polymer was around 50 nm thick. The lighter-coloured areas in picture (a) of Figure 12 are the areas where the polymer could not adhere to the silicon base. The deposited PFDA layer is roughly 100 nm thick. The surface defects appear as bright spots in the coating in picture (b) of Figure 12.

These surface defects tended to be bigger in the thin V4D4 base coating with a diameter of roughly 20 µm. In the slightly thicker PFDA coating, the surface defects were much smaller with a diameter of roughly 3 µm. No surface defects were visible in the copolymer layer, which is around 300 nm thick.

The surface defects could be due to insufficient cleaning and drying of the wafers before the depositions or due to expired monomers. The monomers were changed out for fresh ones after the surface defects were discovered. The biggest defects appeared in the thinnest coatings, while the thickest coatings showed no sign of the same imperfections.

During the cleaning process, the wafers are blow-dried with CO_2 gas. If the compressed gas gun is held too closely to the wafers during the drying process, air, gas or oil from the compressor could condensate on the surface of the cleaned wafers and add contamination to the cleaned surface again. After this was discovered and the distance from which the

wafers were dried was adjusted, the subsequent depositions did not show any surface defects in the coatings.

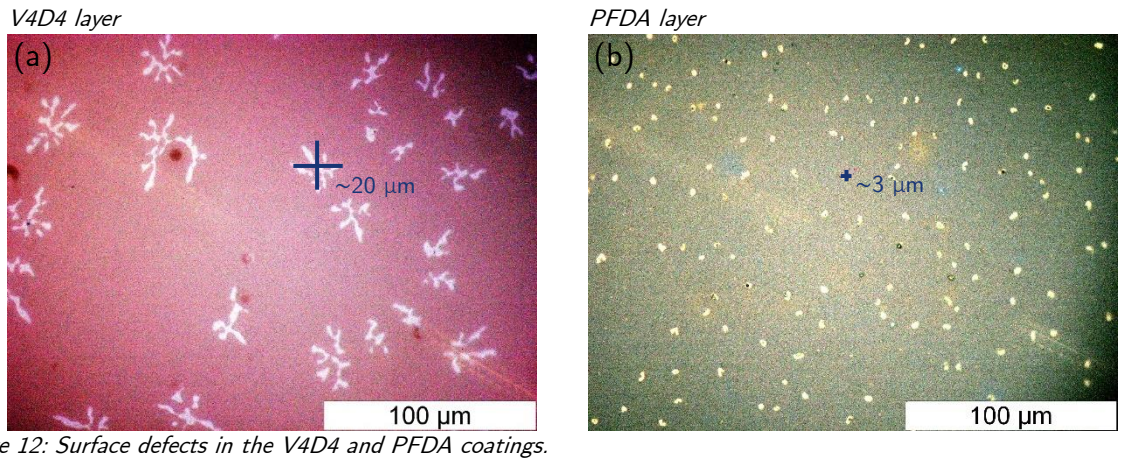

Figure 12: Surface defects in the V4D4 and PFDA coatings.

4.2 Coating thickness measurement

Ellipsometry was performed on the reference samples after the depositions to measure the height of the coatings of the patterned samples. Ellipsometry requires a large uniform surface area in order to adequately measure the thickness of surface coatings. The patterned samples had surfaces, that were too rough to perform ellipsometry, hence atomic force microscopy was used to further investigate the thickness of the coatings of the patterned samples. The measurements were performed at room temperature in ambient air. The thickness measurements were achieved by setting a 1.50 nm thick base layer of SiO_2 and then calculating the coating thickness using a Cauchy model.

The coating thicknesses measured with ellipsometry showed that the reference wafers had coatings in roughly the desired thicknesses, as shown in Table 3. The PFDA dots on the V4D4 base had a combined thickness of roughly 100 nm. The copolymer dots on the silicon base were roughly 300 nm thick.

The coating thickness can be measured in situ during the iCVD reactions. The duration and speed of the deposition can be adjusted accordingly. The interferometer measurements are a good indicator, but the coating thickness can be influenced by a few things, like the placement of the samples in the reactor or user error when the reaction is stopped too early or too late.

The average coating thicknesses of the different polymers are listed in Table 3. The thicknesses of the unpatterned reference wafers were higher than the desired coating thicknesses. The PFDA and copolymer layers were a lot thicker than the desired coating height. The reference wafers were placed closest to the monomer inlets, and no mask was placed on them, which could impede the monomers from polymerizing on the sample surface.

Table 3: Overview of the desired and measured coating thicknesses of the unpatterned wafers.

Sample	Measured polymer coating thickness	Desired coating thickness
Patterned hydrophobic surface: V4D4 base layer with PFDA dots		
V4D4 base layer	52.29 ± 3.68 nm	50 nm
PFDA top layer	150.29 ± 32.25 nm	100 nm
Patterned biphilic surface: Silicon base with copolymer dots		
Copolymer layer	405.77 ± 20.22 nm	300 nm

4.3 Pattern height determination

Atomic force microscopy was performed on the samples to measure the height of the coatings. During the iCVD deposition, the thickness of the coatings was measured with an interferometer on unmasked silicon wafers. This allows for the depositions to be in the approximate thickness range and the iCVD reaction to be stopped at the right time.

The in situ height measurement is performed on unmasked silicon wafers because the mask interferes with the laser signal. The samples are all masked and placed further away from the monomer inlets, which could lead to a lower coating thickness.

The pattern height measurements were performed at room temperature and in ambient air. The pictures were analyzed with Gwyddion.

4.3.1 Pattern height measurements

After the samples were removed from the reactor and cleaned, the height of the patterned dots was measured by atomic force microscopy (AFM). The largest potential area to be

examined was 70 by 70 µm. The smallest patterned dot has a diameter of roughly 100 µm. This means, only parts of the patterned dots are visible in each picture.

Atomic force microscopy on the samples with a plain silicon base and 0.1 mm copolymer dots shows the two easily distinguishable regions, which are depicted in Figure 13.

In the picture (a) of Figure 13, the plain silicon base is the darker area on the left side. The brighter regions in the AFM picture are the areas that are raised. The lighter area on the right side is the surface of the copolymer dot, which is elevated in comparison to the silicon base. Surface defects are visible along the edge of the dot, on the silicon base and on the copolymer surface. These are raised areas and they appear as very bright spots in the picture. A big surface defect can be seen on the silicon base in the top left corner of picture (a). This could be an area where the monomers leaked under the mask during the deposition or any other type of particle. Glue residue left behind after cleaning or dust particles could also lead to surface defects.

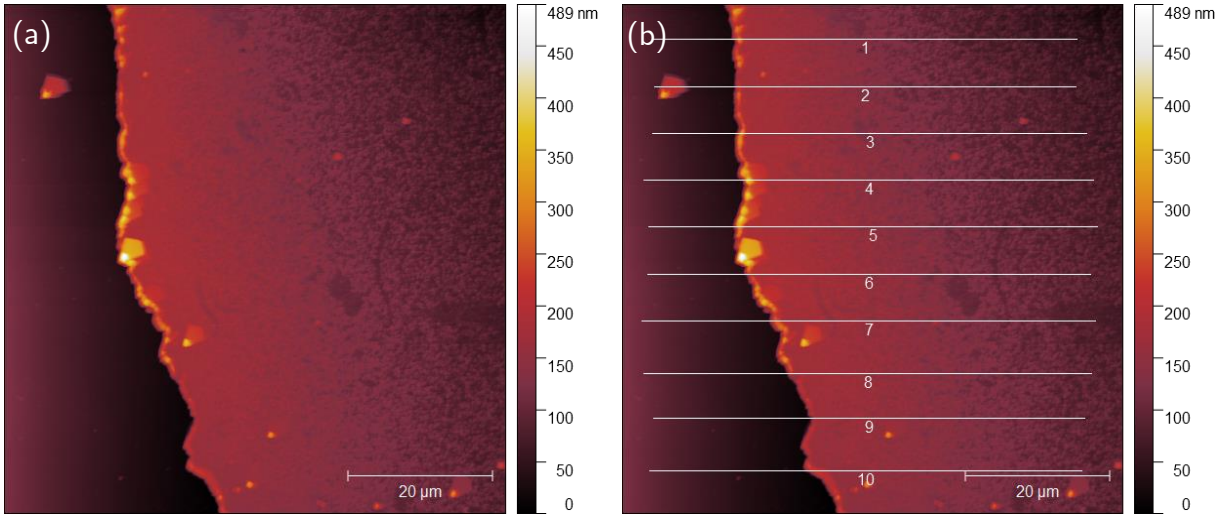

Figure 13: (a) Atomic force microscopy picture of the topography of a gradient copolymer dot on a silicon base and (b) the same AFM picture with ten lateral height measurements across the silicon base and the surface of the copolymer dot.

To measure the height of the patterned dot, parts of the base and the edge need to be visible in each picture. To evaluate the elevation difference, both regions, the base and the dot surface, need to be visible. After the pictures were taken, the tilt of the sample was adjusted. For each of the 10 measurements shown in Figure 14, a baseline was set that corresponds to the base coating of the sample. This baseline was then subtracted from the total height measurement to bring all height profiles to the same base layer height. The V4D4 baseline is the green line in Figure 14.

To determine the height difference between the base and the patterned dots, ten lines were placed across the total area of the AFM picture as seen in picture (b) of Figure 13 and the height difference was measured. The surface defects are the small but high peaks in the height profile line. The average height difference between the silicon base and the copolymer dot on this sample was around 200 nm. The black line in Figure 14 indicates the average height of the ten measurements. The height of the dot is lower than expected, but the patterned dots are distinguishable raised areas on the surface of the sample.

Usually, there are surface artifacts around the edge of the dot. This could be because of the breaking of the conformal coating when removing the mask. The monomers deposit not only on horizontal but also on vertical planes during iCVD reactions. When the mask is peeled off, the polymer coating breaks, leaving behind jagged structures around the dot edge. High spikes in the coating thickness around the breaking points of the polymer can be expected.

The height of the coating along the edge is lower and rises towards the middle of the dot. The highest coating thickness was measured on the edge of the AFM picture, closer to the middle of the dot. This could be because the mask inhibited the monomers from uniformly depositing close to the edge of the mask or because of the baseline adjustments of the AFM pictures.

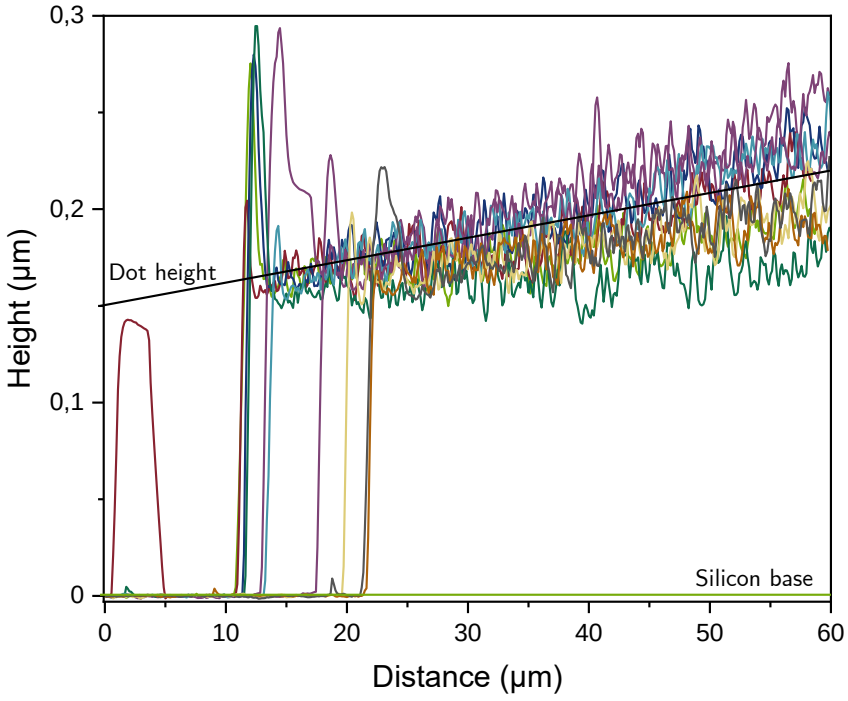

Figure 14: Height profiles of the ten lateral measurements across the silicon base and the copolymer dot.

4.3.2 Pattern height results

The expected deposition thickness for the dots of the hydrophobic pattern is 100 nm. To measure the height difference between the V4D4 base layer and the PFDA dots, AFM pictures of the surfaces with the three different pattern sizes were taken and ten lines along which the elevation was recorded were placed in each picture. The average height difference of the dots and the standard variance was calculated. The surface defects along the edges of the dots were excluded from the height calculations. To calculate the average coating thickness, at least three different dots per pattern were measured with AFM and at least 30 different height measurements were taken.

On average, the measured height difference was 96 nm, which was a little lower than the expected 100 nm. Except for the 0.5 mm dot patterned surface, all the measured PFDA deposits were under 100 nm. The results are listed in Table 4. This could be because of the placement of the masked wafers in the iCVD reactor. Samples placed further away from the monomer inlet have a lower coating thickness than the samples placed in closer proximity to it. The mask might also initially inhibit the monomers from reaching the sample surface by redirecting the monomer flow across the sample surface. The mask might also prohibit the reactor heating or the cooling stage from regulating the sample temperature properly, thus delaying the coating of the sample.

The expected deposition height for the dots of the biphilic pattern is 300 nm. The measured copolymer dot heights were on average 219 nm. This is much lower than the expected coating thickness. Again, this could be due to the placement of the samples in the reactor or the mask interfering with the deposition.

Even though both measured coating thicknesses were lower than predicted, the iCVD depositions led to clearly defined coated areas on the samples. The shape of the pattern and abrupt height differences have been observed.

Table 4: Overview of the patterned dot heights

Sample	Measured the height of the dots	Deposited dot height
Patterned hydrophobic surface: V4D4 base layer with PFDA dots		
0.1 mm dots	84.32 ± 15.56 nm	100 nm
0.5 mm dots	113.52 ± 17.61 nm	
1 mm dots	88.90 ± 26.54 nm	
Overall average: hydrophobic surface	95.58 ± 19.9 nm	
Patterned biphilic surface: Silicon base with copolymer dots		
0.1 mm dots	235.84 ± 35.72 nm	300 nm
0.5 mm dots	229.66 ± 30.88 nm	
1 mm dots	181.60 ± 12.91 nm	
Overall average: biphilic surface	218.58 ± 27.82 nm	

4.3.3 Dot profile investigation

The atomic force microscopy machine could only take pictures up to 70 by 70 µm. It was not possible to take a picture of an entire patterned dot. To investigate the complete profile of a patterned dot, multiple pictures in sequence are necessary. Four pictures were taken next to each other, spanning from the base layer across the patterned dot to the other side to create a full side profile overview. The process is detailed in Figure 15.

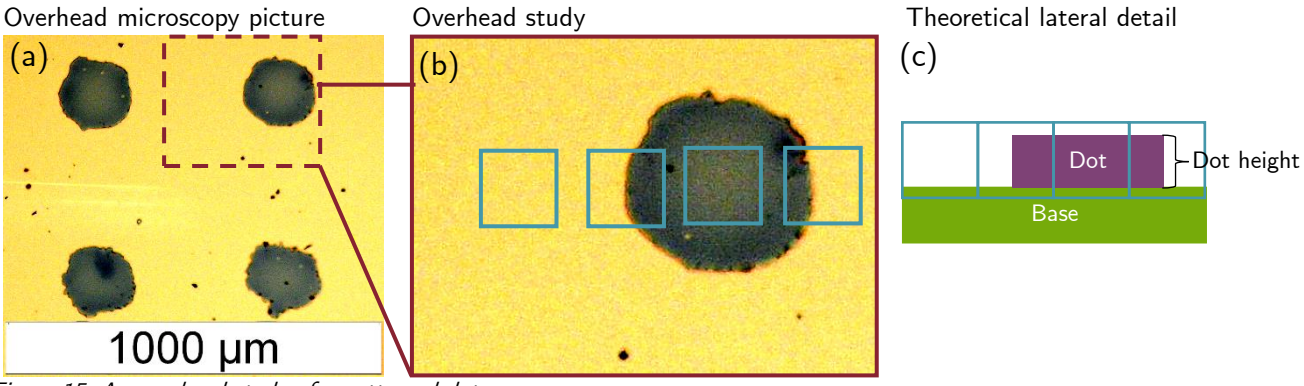

Figure 15: An overhead study of a patterned dot

The first graph, graph (a) of Figure 16, shows the V4D4 base layer. It is quite level, with a few distinct disturbances on the flat surface. The surface artifacts can be holes or valleys in the V4D4 coating as well as surface artifacts that stick out from the surface.

Graph (b) shows the left edge of the patterned dot. Around the edge of a dot, a lot of surface artifacts are visible, but also on the V4D4 base layer, as sharp and high peaks in the height measurements. Next to the surface artifacts, the coating thickness of the patterned dot is lower before it starts to rise again toward the middle of the dot.

Graph (c) shows the surface of the PFDA dot. There are a lot of fine surface artifacts visible in this coating. The height measurement shows a lot of fine peaks and valleys. This means the surface is quite rough. Only a few distinct tall peaks are visible and a few deep holes were measured. At these points, the surface coating is not as thick.

Graph (d) shows the right edge of the patterned dot. The coating thickness decreases from the middle of the dot towards the edge. This could be because of the tilting of the sample and the baseline adjustment of the height profiles. Surface artifacts at the edge of the dot and holes in the V4D4 base layer are visible.

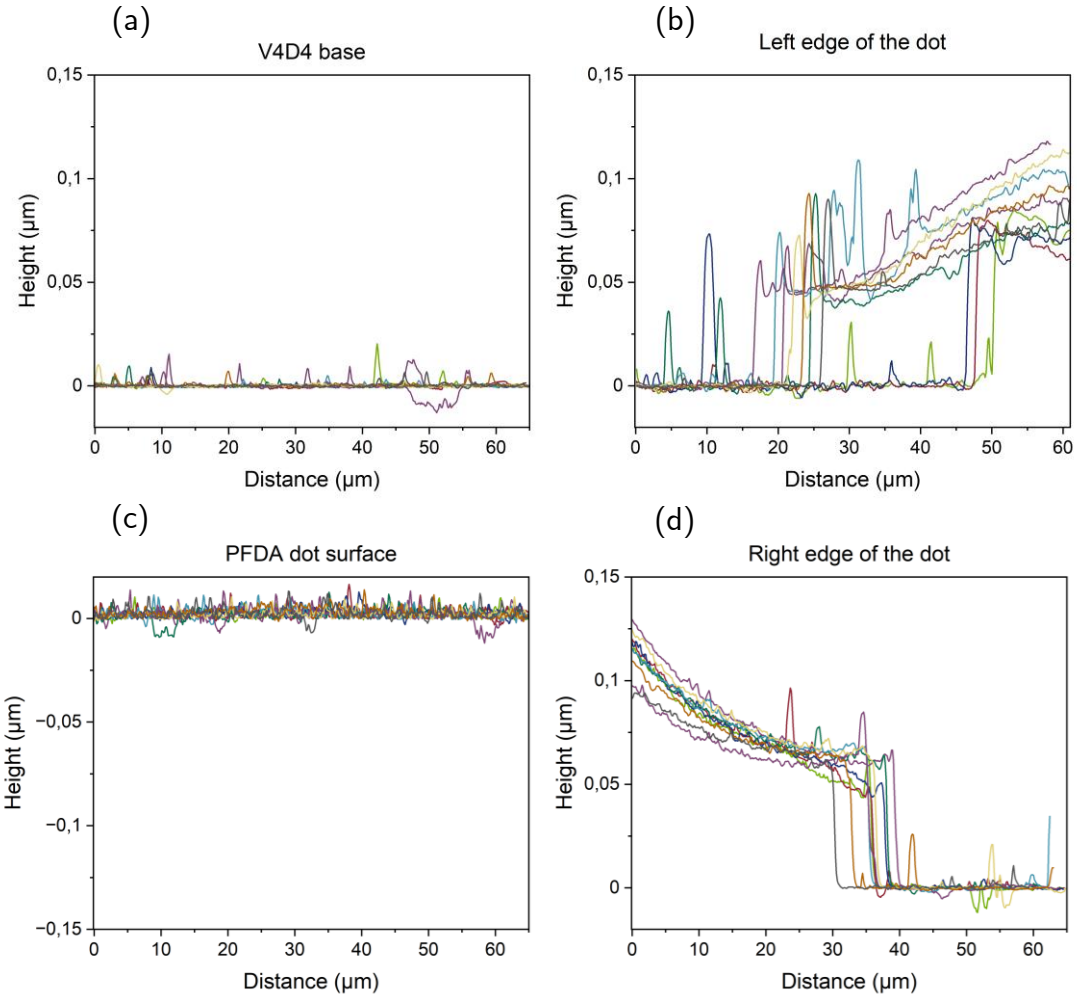

Figure 16: Side profile of a PFDA dot on a V4D4 base.

The same side profile pictures were taken of a copolymer dot on a silicon base.

Graph (a) of Figure 17 shows the silicon base, which has very few defects. Only a few surface artifacts are visible.

Graph (b) shows the left edge of the copolymer dot. The silicon base is very flat and the edge of the dot is very steep. Along the edge of the dot, a lot of surface artifacts are visible. Behind the surface defects along the dot edge, the thickness of the coating is lower but starts to increase again closer to the middle of the dot. This could be because of the mask inhibiting a uniform deposition during iCVD or because of the baseline adjustment of the pictures.

The third graph, graph (c) shows the surface of the copolymer dot. The copolymer has a rough surface compared to the silicon base. The rough surface is a characteristic of the gradient copolymer used. [19], [20]

Graph (d) shows the right edge of the dot. Steep surface defects are visible along the edge. The coating thickness of the dot decreases towards the edge of the dot while the silicon base is very flat with only a few surface defects.

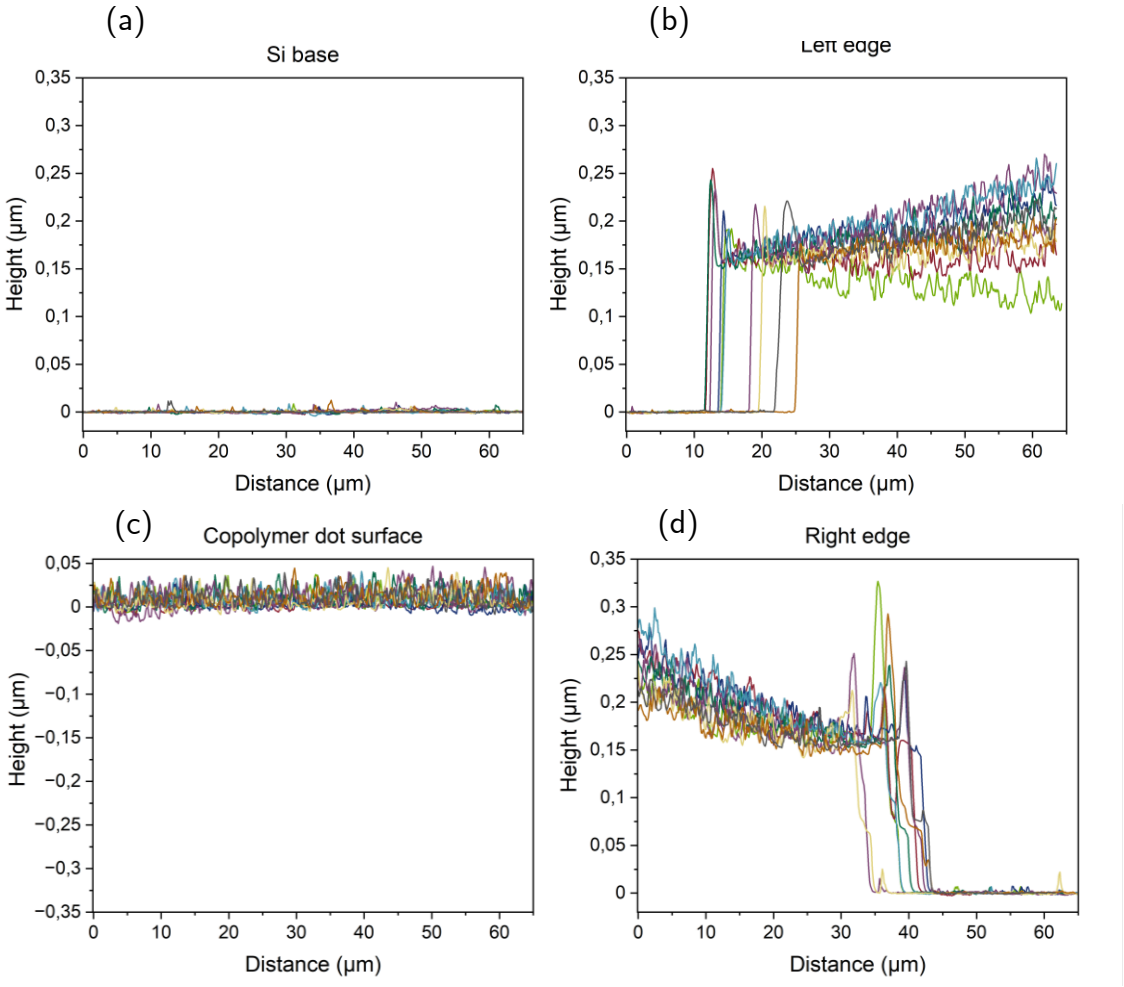

Figure 17: Side profile of a copolymer dot on a silicon base.

4.4 Wettability

Water contact angle measurements were performed on all the samples. The measurements were done with 5 µl distilled water at room temperature in ambient air. For each sample, five drops were placed on their surface, the left and right contact angles were measured with a goniometer and the average was calculated.

For the hydrophobic surfaces, the water contact angle was measured on an unpatterned surface of V4D4, an unpatterned surface of PFDA and the three different patterned surfaces and an unpatterned silicon wafer as a reference. V4D4, the base coating, is slightly hydrophobic. PFDA, the coating of the dots, is more hydrophobic. Silicon, the base for all the coatings, is hydrophilic.

Figure 18 shows that, as expected, the water contact angles for the patterned surfaces using those two polymers were between the water contact angle values of the unpatterned surfaces coated with each of these two polymers. The water contact angles do not vary a lot between the different pattern sizes. When regarding the variance, all the patterns had roughly the same water contact angle range.

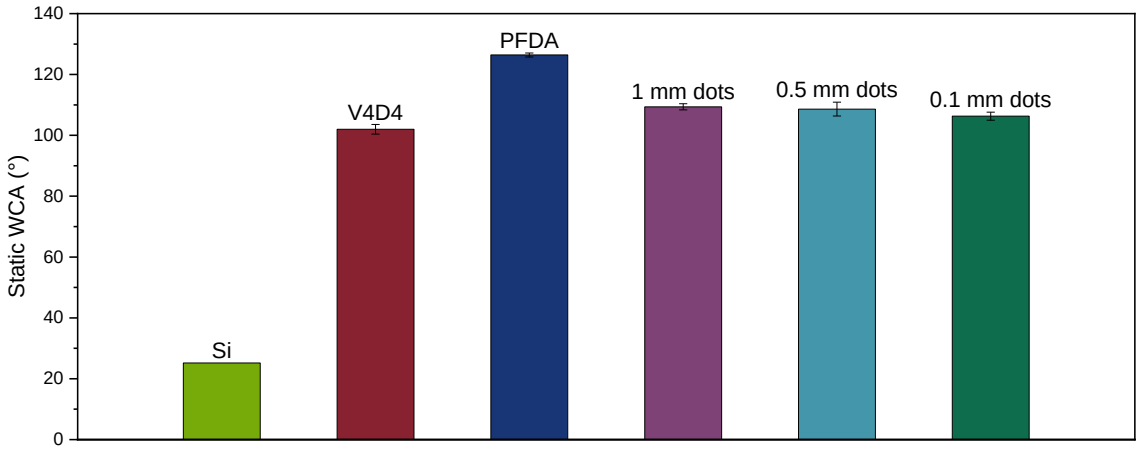

Figure 18: Static water contact angle measurements of the patterned hydrophobic surfaces in comparison to silicon and unpatterned V4D4 and PFDA surfaces.

For the biphilic surfaces, the water contact angles of an unpatterned surface coated with the copolymer, plain silicon and the three different patterned surfaces were measured.

The copolymer-coated surface has a very high-water contact angle of over 125° while the plain silicon, which is hydrophilic, has a very low water contact angle. The patterned surfaces all had water contact angles around 80 to 90°, they were not or not significantly hydrophobic.

The water contact angles increase with decreasing dot size. Of note is that the biggest pattern had the lowest water contact angle. The 1 mm pattern also has the biggest surface coverage of the copolymer dots. The waterdrops were 5 µl and touched the patterned dots and the base layer on every patterned surface. The waterdrop surface area was significantly larger than the patterns. With decreasing pattern size, the water contact angles increased. The smallest pattern had the highest water contact angle, even though only roughly 13% of the surface was covered with a hydrophobic copolymer. On the surface with the smallest pattern, the waterdrop was in contact with a lot more hydrophobic dots, which seemed to increase the water contact angle.

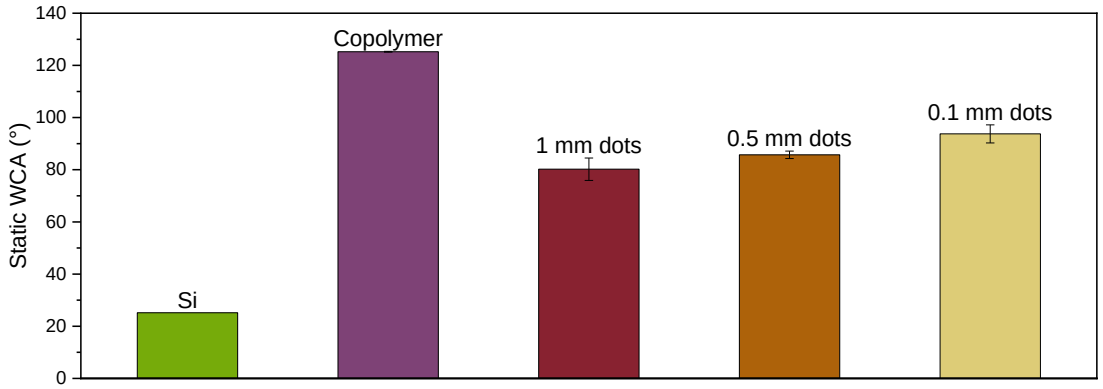

Figure 19: Static water contact angle of the patterned biphilic surfaces in comparison to silicon and unpatterned copolymer surfaces.

The waterdrops behaved differently depending on which surface they were placed. The water contact angle measurements for the hydrophobic parts were similar for both edges of the drop, while the measurements for the biphilic surfaces would vary depending on what parts of the biphilic surface the edges of the drops were located. [5], [23]

Water contact angle measurements on a starburst pattern were not possible because the water just moved off of the hydrophobic onto the hydrophilic area. Because the drops tended to move from the hydrophobic pattern to large hydrophilic areas, the starburst pattern was not selected as a patterning technique for the ice nucleation and frost propagation tests.

4.5 Roll-off angle

The roll-off angle was measured to examine the behaviour of waterdrops when the samples were tilted. A static waterdrop of 18 µl distilled water was placed on the sample surface before it was tilted to 90°. The angle necessary for the waterdrop to roll off was noted. The experiment was conducted at room temperature in ambient air. The measurements were repeated three times, and the average was calculated.

The biphilic patterned surface did not have a roll-off angle, which is listed in Table 5. The waterdrops did not roll off. Even at a 90° tilt angle, the waterdrops stayed on the sample surface. During some experiments, the drops seemed to move slightly, but after tilting the samples back into the horizontal plane, the waterdrops moved back to their starting place.

The silicon base of the biphilic wafers is hydrophilic, while only the patterned copolymer dots are hydrophobic. The waterdrops are big enough to cover multiple dots and the base layer when they are resting on the surface. The structured copolymer dots in a grid pattern and the silicon base seem to lead to the drops sticking to the surface, even at large tilting angles.

The drops on the hydrophobic patterned samples had a very high roll-off angle. The smallest pattern with 0.1 mm dots had the largest roll-off angle, while the biggest pattern with 1 mm dots had the smallest roll-off angle. The smaller pattern led to the drops staying on the samples up to higher tilt angles. The edges of the patterned dots seemed to provide anchors for the waterdrops.

Even though some of the prepared surfaces were hydrophobic, the waterdrops did not roll off easily. The water contact angle of the drops on these surfaces is high, but this does not have to translate to a low roll-off angle. Hydrophobic surfaces can lead to a pinning effect. Water placed on them is held in place, even at high tilting angles. The magnitude of adhesion can be high on hydrophobic surfaces, especially on the edges of the patterned dots. [24] Air trapped in the irregular shapes of the surface can lead to high adhesion forces like the Magdeburg hemispheres. At high tilting angles, the air pockets that are fully covered by the waterdrop exude high attraction forces. [25]

Table 5: Overview of the roll-off angles of the different samples

Sample	Roll-off angle
Patterned hydrophobic surface: V4D4 base layer with PFDA dots	
0.1 mm dots	81.55 ± 9,07°
0.5 mm dots	81.05 ± 6,57°
1 mm dots	59.32 ± 2,08°
Patterned biphilic surface: Silicon base with copolymer dots	
0.1 mm dots	---
0.5 mm dots	---
1 mm dots	---

5 Icephobicity tests

Two different types of experiments were conducted to evaluate the anti-icing abilities of the created surfaces. One experiment was an ice nucleation test where waterdrops were placed on the surfaces and then cooled down to temperatures below the freezing point of water. The time it took for the waterdrops to freeze was measured. The second set of experiments performed were frost propagation tests. The samples were cooled to temperatures below 0° while the water condensation and frost propagation across them were observed under a microscope. Combined, these experiments give an overview of how the samples behave in cold conditions and if they have icephobic abilities.

5.1 Ice nucleation tests

To see if the patterned surfaces delay the ice formation ice nucleation tests were performed. The time it takes for water to freeze on cooled samples is investigated. The measurements of the ice nucleation delay times of the different types of patterned surfaces are then compared to a silicon surface and their matching unpatterned surfaces. These experiments were done in a similar way as other research groups have performed their ice nucleation experiments. [19], [26], [27]

The measurements were performed at ambient humidity, starting at room temperature, and cooling down to the measurement temperature. The average humidity during the tests was 30%. The measurement temperatures were -15, -20, -25 and -30°C.

5.1.1 Ice nucleation test setup

The samples were placed on a cooling stage below an infrared camera in an environmental chamber. The humidity in the environmental box was the ambient humidity in the lab. For each measurement, five waterdrops were placed on the sample surface. One drop was placed in the middle and four drops were placed close to the four corners of the samples. They were video-monitored and their temperatures were

measured. The video was recorded on a laptop. The humidity inside the environmental chamber was recorded and could also be read from a monitor.

The cooling stage settings could be adjusted with the control board. There the temperatures the sample should be cooled down to could be set as well as how fast and how long it should be cooled. Liquid nitrogen in a Dewar was used as a cooling agent. A small pump is submerged in the liquid nitrogen and pumped it from the Dewar to the cooling stage. A water cooling and heating system was used to control the temperature of the samples in tandem with the liquid nitrogen, and it was responsible for warming the sample back up to room temperature after the tests were completed.

After the measurements were done, the samples were warmed up to room temperature until the ice melted. Then the samples were taken out of the environmental chamber, the water was blown off and the samples were dried with air before the experiment was repeated.

For the experiments, the samples were placed on a cooling stage and five 10 µl drops, four in the corners and one in the middle, were placed on the surface.

Then the temperature was reduced to a certain point and the time until all drops froze was measured. The tests were repeated to get 30 measurements for each type of surface and the average freezing delay and the standard variance were calculated. The tests were done at ambient relative humidity, which was on average around 30%. The tests were done for the temperatures of -15, -20, -25 and -30°C to see how the coating behaved with decreasing temperatures.

During the measurements, the waterdrops on the edges of the samples tended to freeze earlier and the ones in the middle tended to stay liquid the longest. Usually, frost would form on the edges of the sample and creep inwards across the surface. Once the waterdrops on the edges were frozen, dendrites, which are frost spikes, formed and frost spread across the surface towards the middle of the samples. [28] The frost propagation can be influenced by changing the humidity in the environmental chamber during the measurements.

5.1.3 Ice nucleation measurements

Figure 20 shows what the temperature settings during measurements looked like. The temperature was reduced from room temperature to the desired measurement temperature. At this point, the time measurement was started. The water was supercooled and it would eventually freeze. The ice nucleation time was of interest. Once

the droplet froze, there was a spike in the observed temperature. Initially, an ice seed crystal forms before it recalesces and spreads through the whole drop. Because of the rearrangement of the atoms in the water when it becomes ice, latent heat is released. This is the exact moment the drop freezes. There was a brief delay of less than a full second until the whole drop was frozen through before the measured temperature started to drop again. [26]

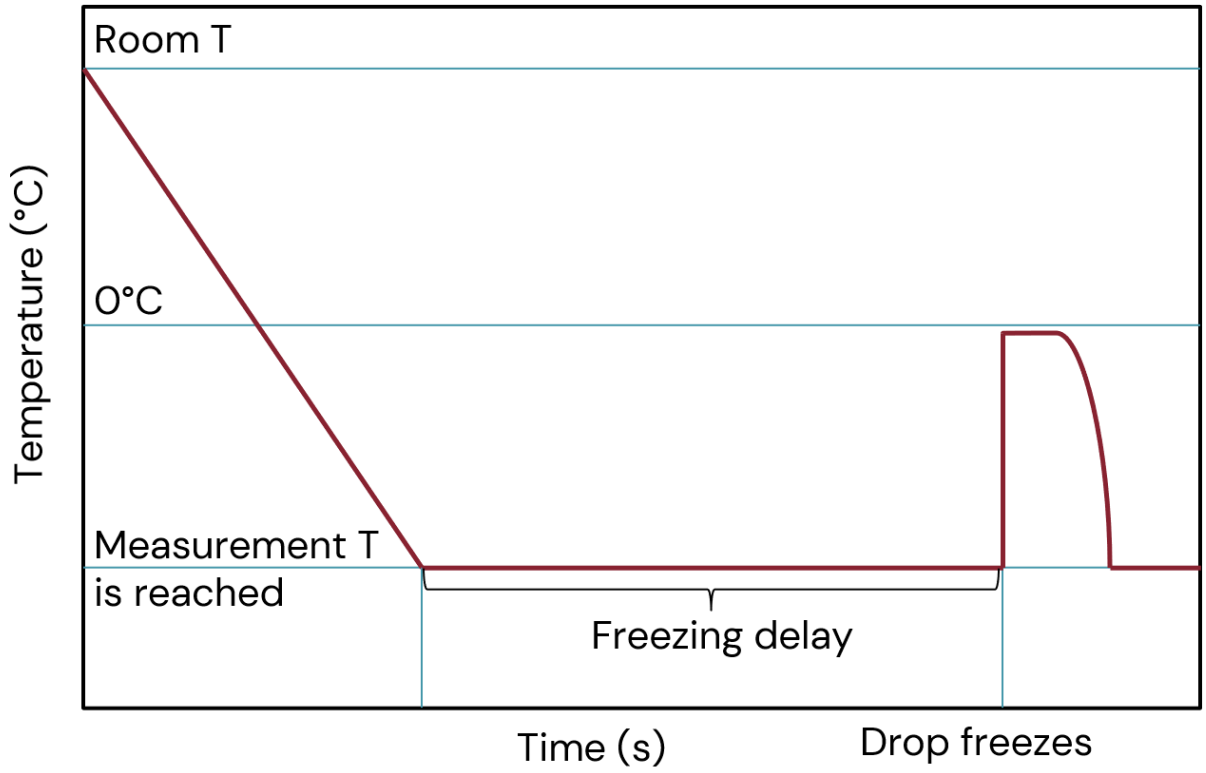

Figure 20: Scheme of the waterdrop temperature during the icing test.

When the drop was placed on the hydrophobic parts of the sample surface, it had a spherical dome shape. Once the waterdrop started to freeze, usually ice started to form on the bottom of the drop, where the supercooled liquid came in contact with the cooled sample surface on the cooling stage. The whole waterdrop froze, the water becoming ice throughout the whole drop, changing its shape because the ice takes up more space than the water. Once the whole drop is frozen through, the drop shape is not a dome shape anymore. It had a spire-like structure on top of a dome. [27]

Figure 21 shows what the measurement data looked like. The time is on the x–axis and the temperature is on the y–axis. A drop was placed on the sample surface and its temperature was measured. The sample was cooled down to -15°C. Once -15°C was reached, the time measurement was started. The spike in the curve indicates the moment

the drop freezes. The time it takes the drop to freeze once the measurement temperature is reached is the freezing delay. [26] It can be seen in Figure 21 that this drop froze after around 55 seconds. The freezing delays of 30 drops per sample were measured, and the average was calculated for each surface.

Usually, the drops placed closer to the edge of the sample froze first. Surface artifacts and damage in the coatings can lead to water adhering to the surface and ice forming faster. Dendrites formed on the frozen drops and gradually frost tended to creep across the surface. Once the frost reached the next waterdrop, the drop tended to freeze faster. When the humidity was low and not a lot of water from the ambient air condensed on the sample surface, the waterdrops tended to stay liquid for longer. [4], [28]

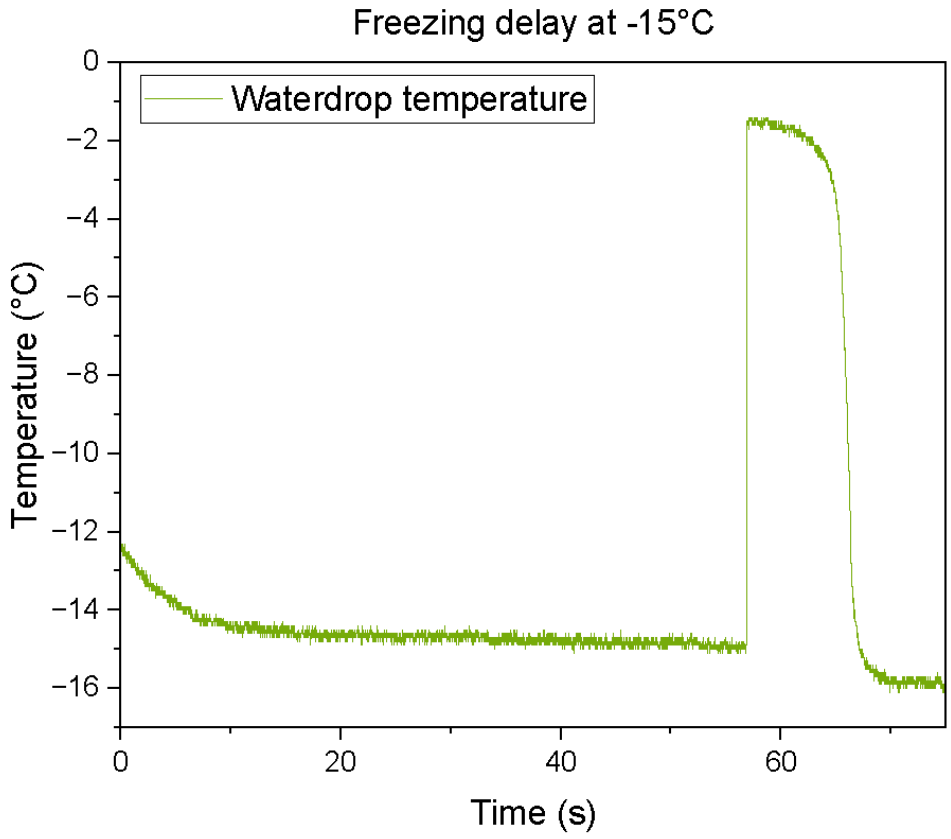

Figure 21: Waterdrop freezing delay.

5.2 Frost propagation

To observe how fast frost spreads across the patterned surfaces, frost propagation tests were performed. The samples were cooled to the measurement temperature and the frost propagation was observed and analyzed. The total frost propagation measurement time was between five and seven minutes. The difference in the frost propagation times of the hydrophobic and the biphilic patterned surfaces was observed. [28], [29]

Frost propagation tests were done at room temperature and at ambient humidity, which was at an average of approximately 20%. The samples were cooled down to -20°C. The test was repeated three times per sample, and the averages and the standard variance were calculated.

5.2.1 Frost propagation setup

For the frost propagation measurements, the samples were placed on a cooling stage under an optical microscope in ambient air. Water out of the ambient air condensed on the cooled sample surface. [23] It took some time until the small waterdrops froze. The time measurements were started once ice crystals were visible in the area observed with the microscope. The experiments were stopped approximately five to seven minutes after the first ice crystals formed, then the entire surface was covered in a layer of frost. The frost propagation speed across the surface was measured, not the delay time until the ice crystals formed. These two mechanisms can work completely independently from each other.

5.2.2 Frost propagation measurements

The samples were placed on a cooling stage that was cooled down to -20°C. The optical microscope was focused on the water condensing on the sample surface. A video recording of the frost propagation was taken, which was later analyzed to calculate the frost propagation speed and surface frost coverage depending on the time. Only the frozen waterdrops were counted. Liquid waterdrops and areas without any ice did not count towards the frosted-over area.

Figure 22 shows a comparison between a patterned hydrophobic surface in picture (a) and a patterned biphilic surface in picture (b), two minutes after the frost propagation started. The areas in the yellow circles are the patterned dots. All waterdrops on the sample

surfaces are frozen. The waterdrops condensing on the hydrophobic surface tended to be smaller, while the waterdrops on the hydrophobic surface were larger. During the observation, the waterdrops on the biphilic surface favoured the hydrophobic silicon base, leaving more uncovered surface area on the hydrophobic copolymer dot. The number of waterdrops on the hydrophobic surface was larger and their size was smaller.

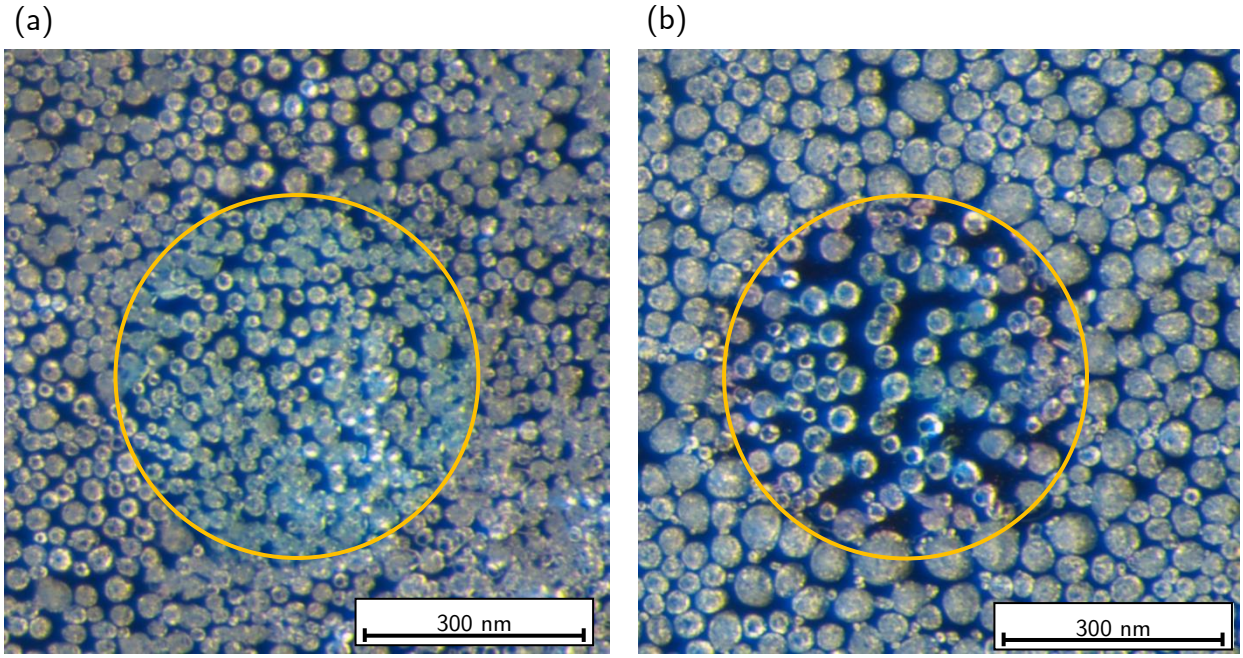

Figure 22: Comparison between a 0.5 mm patterned hydrophobic and patterned biphilic surface after 120 seconds of frost propagation.

Figure 23 shows the spread of the frost across a sample surface over 140 seconds. The sample was biphilic, with a silicon base and 0.5 mm copolymer dots.

The yellow circles indicate the area of the patterned dots. The red line indicates the border between frozen and liquid waterdrops. When the temperature of the sample is reduced, water from the ambient air condenses on the sample surface.

In the beginning, the frost started to spread across the surface from the left side. After 40 seconds, frost can also be seen spreading from the top and the right side growing towards the middle of the sample. The waterdrops on the silicon base tended to freeze earlier while the copolymer dot stayed frost-free for longer, which can be seen in the picture from 60 to 100 seconds. Finally, all the waterdrops across the entire surface are frozen. There are still surface areas visible that are ice-free.

Pictures of the video recording were taken every 10 seconds and analyzed with ImageJ to calculate the percentage of the surface that was covered by frozen waterdrops.

After the measurements were done, the samples were removed for the cooling stage and left to warm back up to room temperature. When the samples reached room temperature and the ice had melted, the water was blown off with air. The samples were dried, and the experiment was repeated.

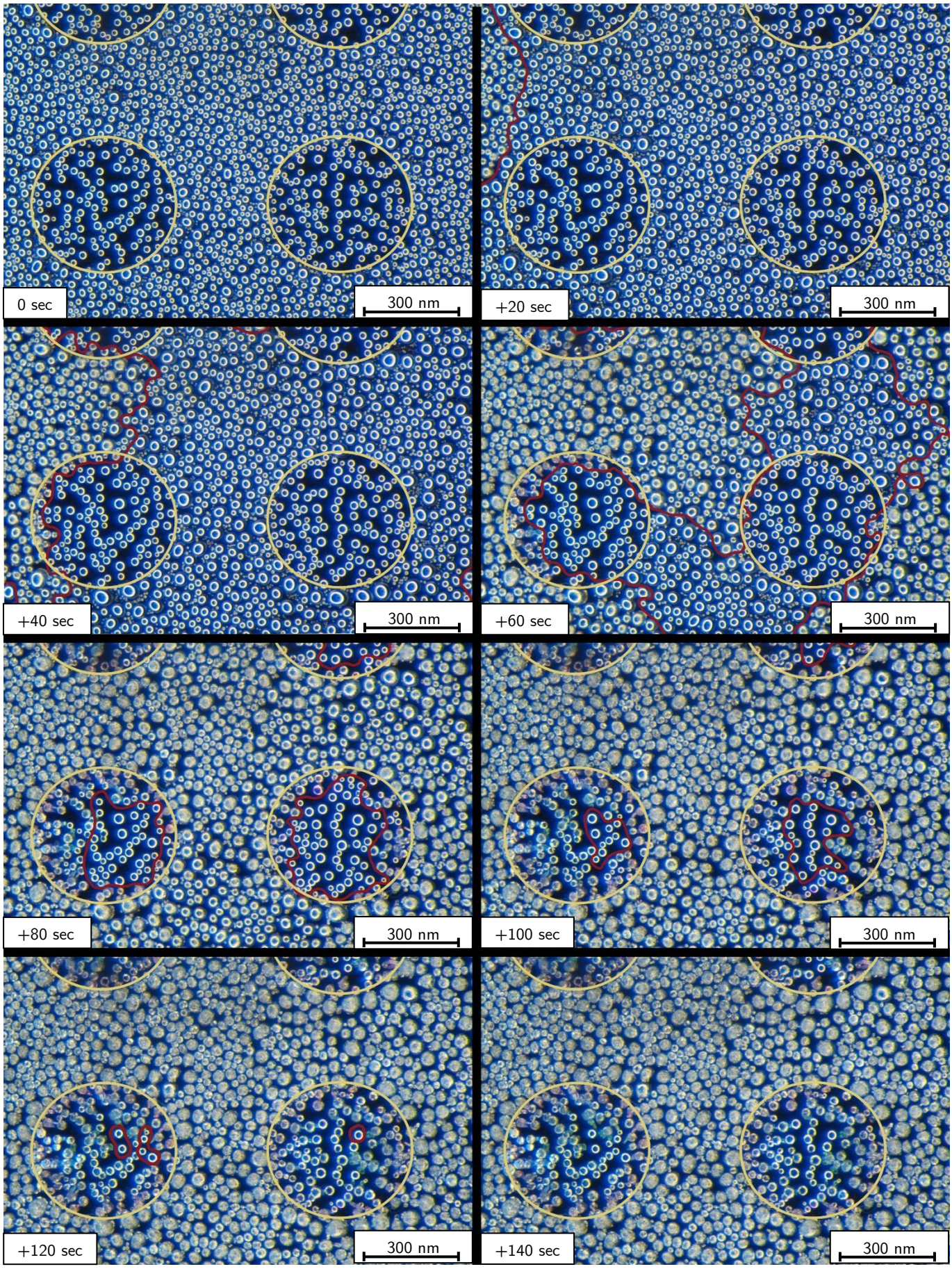

Figure 23: Development of the frost propagation across a biphilic sample surface patterned with 0.5 mm dots.

6 Icephobicity results

This section describes the measurement results of the ice nucleation test and frost propagation measurements.

6.1 Ice nucleation tests

During the ice nucleation tests, the time it takes for ice to nucleate in supercooled waterdrops is measured. The waterdrops can only stay liquid for a certain amount of time on the cooled sample surfaces. Better anti-icing effects lead to longer freezing delays.

6.1.1 Hydrophobic surfaces

Figure 24 shows the results of the hydrophobic patterned samples with a base coating of the V4D4 and dots of PFDA on it.

The temperatures in Celsius at which the measurements were taken are on the x-axis and the average freezing delay in seconds is on the y-axis, which is on a logarithmic scale.

At a freezing temperature of -15°C, all the samples behaved similarly. The average freezing delay was approximately 85 seconds. The surface of V4D4 led to a shorter freezing delay, while the PFDA surface had a longer average freezing delay than all the patterned samples. With decreasing temperatures, the difference in the ice nucleation delay of the distinct surfaces becomes more visible.

At -20°C, the patterned surfaces with 0.1 and 0.5 mm dots performed similarly to how they did at -15°C. The drops on these surfaces stayed liquid for almost as long as at -15°C. The unpatterned PFDA surfaces had a decreased average freezing delay but still outperformed the patterned samples while the plain V4D4 surface had a drastically reduced average freezing delay. The plain silicon surface had a very short average freezing delay of less than a second below -20°C.

The pattern with the 1 mm dots, the biggest dots and the plain V4D4 surface had a significantly shorter average freezing delay at -20°C. The anti-icing effect of these surfaces seems to sharply decline below -15°C. At lower temperatures of -20°, -25° and -30°C, waterdrops on the 1 mm dots pattern seem to stay liquid for roughly the same amount of time and the average freezing delay only declines marginally. The unpatterned V4D4 surface has a longer freezing delay for -25°C than for -20°C. The ice nucleation is a partially stochastic process. The duration until a waterdrop freezes is somewhat random, explaining why it is possible that the average freezing delay can be longer at lower temperatures.

The surfaces with the 0.1 and 0.5 mm dots and the PFDA surface seem to lose their anti-icing effect below a temperature of -20°C. It can be assumed that the smaller patterns indeed seem to delay the ice formation on the surface down to a certain negative temperature.

At -30°C, the measured average freezing delays seem to differ from each other, but the y-axis is on a logarithmic scale, so the difference between the best and worst performing surface at this temperature was only roughly two seconds.

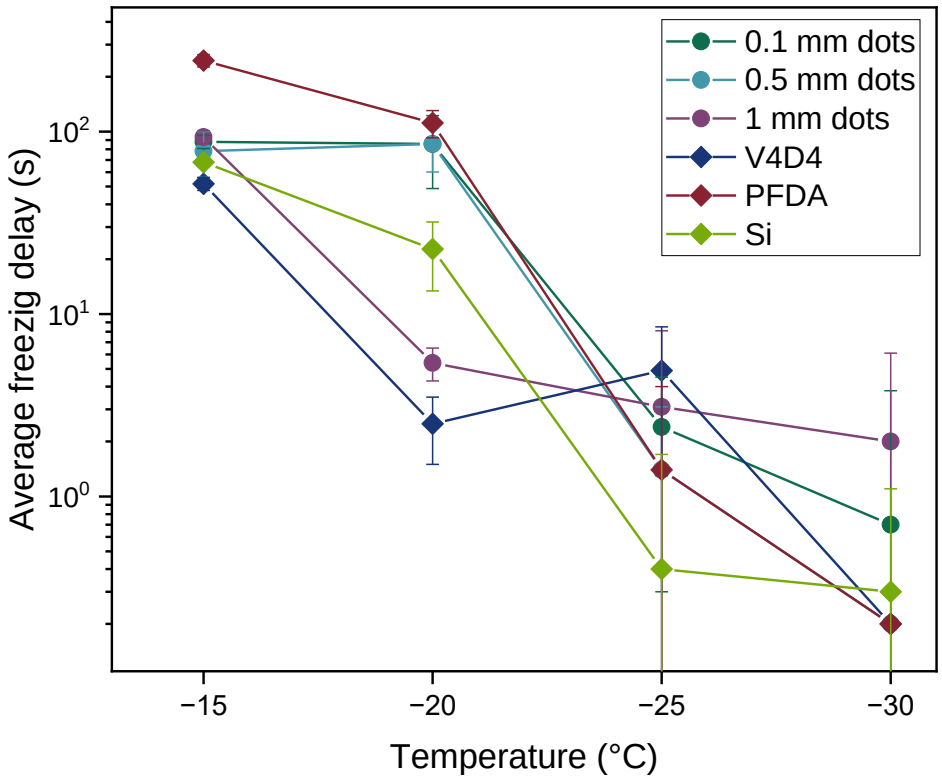

Figure 24: Average freezing delay of the patterned hydrophobic samples and the unpatterned V4D4, PFDA and silicon surfaces at different temperatures.

6.1.2 Biphilic surfaces

Figure 25 shows the results of the samples with copolymer spots on a plain silicon base compared to a plain silicon surface and a plain copolymer surface. The patterned surfaces are biphilic.

At higher temperatures, the patterned surface had a longer average freezing delay than the plain silicon but not as long as the uniformly copolymer-covered surface. With decreasing temperatures, the average freezing delay values tend to spread out, and the average freezing delay times vary a lot between the different patterns.

Once again, the patterned surfaces seem to delay the ice formation quite well up until –20°C below which the average freezing delay times are approximately ten seconds or fewer. The 0.1 mm pattern has a longer average freezing delay at -20°C than at 15°C.

Generally, there is a downward trend in the average freezing delay at lower temperatures, which is to be expected. The patterns with the smallest dots tend to delay icing for the longest, while the water on the surface with the largest pattern tends to freeze earlier. The plain silicon surface performed worse than all the samples, but the plain copolymer surface seems to perform better and delay the ice nucleation for longer than the patterned surfaces at higher temperatures.

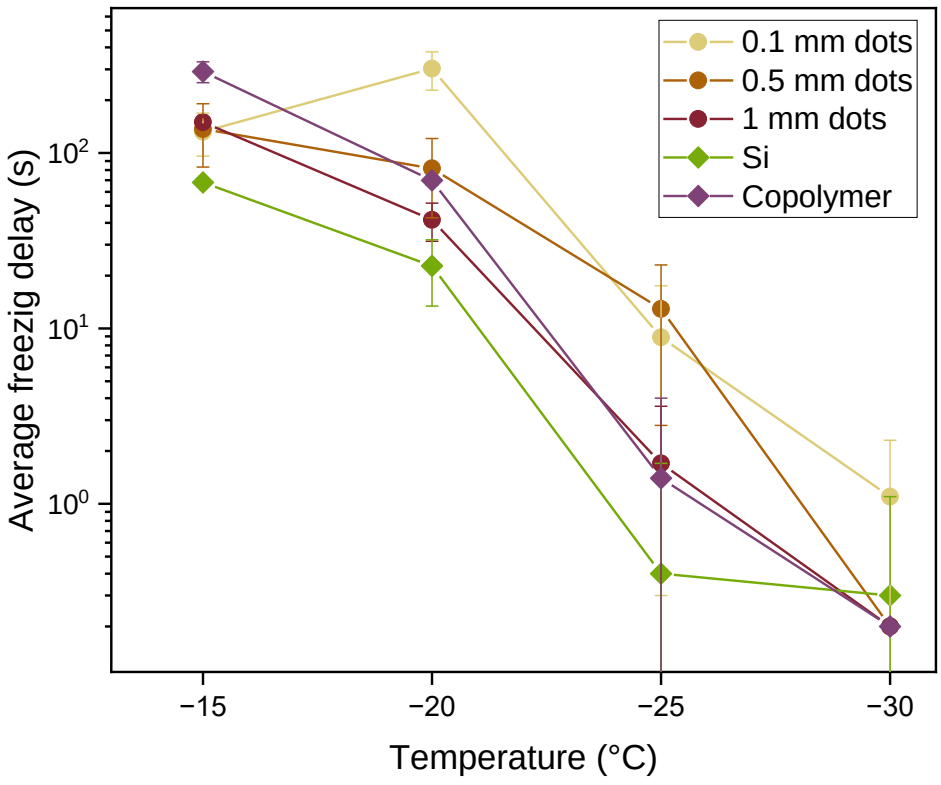

Figure 25: The average freezing delays of the patterned biphilic samples in comparison to unpatterned copolymer and silicon surfaces at different temperatures.

6.1.3 Comparison between the two different surface types

Figure 26 shows a comparison between the samples with a patterned hydrophobic surface and a patterned biphilic surface. The average of all three different patterns of each type of surface at every temperature was calculated and compared to a plain silicon surface and an unpatterned copolymer surface. The silicon surface had the shortest average freezing delay out of all the surfaces that were investigated and the copolymer surface had the longest average freezing delay.

The patterned surfaces seem to delay the ice formation for longer compared to unpatterned plain silicon surfaces. The samples seem to perform best down to temperatures of -20°C below which the average icing delay is drastically reduced. On average, all the patterned surfaces seem to delay the freezing of water on the surface to some degree.

The patterned biphilic surfaces had a longer average freezing delay than the patterned hydrophobic surfaces. The biphilic surfaces had a lower water contact angle, they were less hydrophobic, but on average, the waterdrops on these surfaces stayed liquid for longer. The hydrophobicity of a surface does not have to correlate with icephobicity.

The plain copolymer-covered surfaces, which are also researched at TUGraz [19], seem to perform best at higher temperatures where they have longer average freezing delays. Below –20°C, the patterned surfaces seem to delay the ice formation better than the unpatterned surfaces.

The uncoated silicon surface had the shortest average freezing delay for all measured samples compared to the patterned and unpatterned samples.

The measurements at -30°C indicate that patterned samples are more icephobic because the unpatterned copolymer and the plain silicon surfaces have the shortest average freezing delays. The y-axis is on a logarithmic scale, meaning that the difference between the measured values is below 0.1 seconds and all surfaces performed similarly at this temperature.

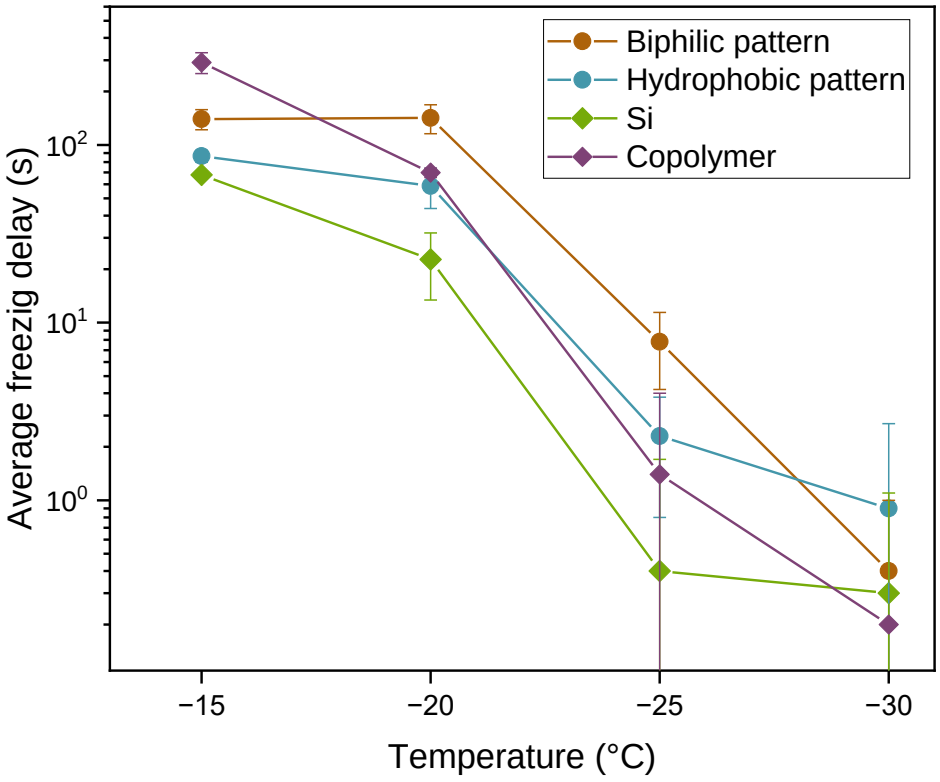

Figure 26: Comparison between the average freezing delays of the patterned hydrophobic and biphilic patterns in comparison to unpatterned copolymer and silicon surfaces.

6.2 Frost propagation tests

During the frost propagation test, the condensation of water from the ambient air onto the cooled sample and the freezing of the drops and the frost propagation are observed. It is expected that the patterned surfaces delay the frost propagation across the surface as well as have an overall reduced frost surface coverage in comparison to an uncoated silicon surface.

6.2.1 Hydrophobic surfaces

Figure 27 shows the ice surface coverage of the patterned hydrophobic samples in comparison to unpatterned V4D4 and PFDA, as well as completely uncoated silicon depending on time.

After 60 seconds, 70% of the plain silicon surface is already covered with frost. The patterned hydrophobic samples had a surface coverage of roughly 20%. The unpatterned samples had a much lower frost surface coverage of below 10%.

The 50% surface coverage point was reached after less than 50 seconds for the plain silicon surface. The patterned samples and the unpatterned V4D4 surface had a 50% frost cover after approximately 100 seconds, while the unpatterned PFDA surface reached the halfway point after close to 200 seconds.

At the end of the experiments, the surface area covered with frost on the plain silicon surface was close to 100%. The patterned samples had a frost surface coverage of around 75% after six minutes while the unpatterned V4D4 and PFDA surfaces had a frost surface coverage of above 80%.

With increasing time, the frost surface coverage of the samples rises. The silicon surface has the fastest frost propagation and the highest frost surface coverage at the end of the experiments. At the beginning of the experiment, the patterned samples have a faster frost propagation than the unpatterned samples. After six minutes, the surface coverage of the patterned samples was lower than the one of the unpatterned samples.

The three different patterns all behaved very similarly at the beginning. The smaller patterns had a slightly faster frost propagation, but at the end of the experiment, all had a roughly 75% frost cover.

It is important to note that the variance of the calculated values is quite high. While the average frost surface coverage of the patterned samples is lower than that of the unpatterned samples, the variances of the values are quite high. For some experiments, the patterned and unpatterned samples behaved almost identically.

The unpatterned surfaces led to a slower frost propagation at the beginning of the experiments. The unpatterned silicon surface had a much faster frost propagation than the patterned and unpatterned hydrophobic surfaces.

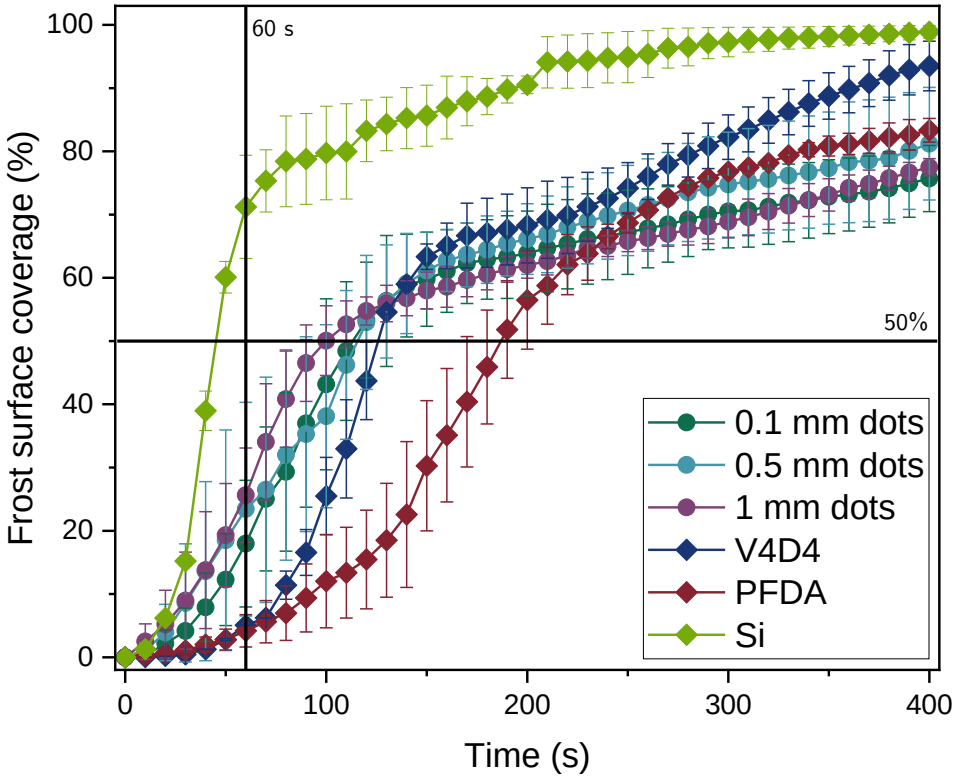

Figure 27: Frost propagation on the patterned hydrophobic samples and unpatterned V4D4, PFDA and silicon.

6.2.2 Biphilic surfaces

Figure 28 shows the frost propagation delay of the biphilic patterned samples in comparison to a plain silicon and an unpatterned copolymer-coated surface.

After 60 seconds, over 70% of the silicon surface is covered with ice. The unpatterned copolymer surface has a frost surface coverage of below 15%. The biphilic patterned samples have roughly 30% surface coverage after one minute. The 0.1 mm and 1 mm patterns have a higher surface coverage of about 40% while the 0.5 mm patterned surface only has a roughly 25% surface coverage. The patterned surfaces had a larger frost surface coverage than the uniform copolymer, but a much smaller surface coverage than the uncoated silicon.

50% of the frost surface coverage of the uncoated silicon surface was reached in under 50 seconds while it took 130 seconds to reach the same frost coverage on an unpatterned copolymer surface. The patterned biphilic surfaces all behaved similarly to each other and needed around 100 seconds to reach 50% frost coverage. The 0.1 mm and the 1 mm patterned surfaces had a faster frost propagation than the 0.5 mm pattern.

An interesting and unexpected result is, that one of the patterned surfaces had a slower frost propagation than the others. It was not the smallest or the largest pattern, but the medium-sized one with 0.5 mm dots. This could be because of the irregular behaviour of the waterdrop condensation and freezing. The standard variance in the experiments is quite high. Repeating the experiments more often would give a better indicator if the 0.5 mm patterned biphilic surface does have a larger average frost delay than the other patterns.

After over six minutes, the silicon surface had an almost complete frost coverage. The copolymer only had a roughly 85% frost coverage. The patterned surfaces also had roughly 85% frost coverage with the biggest pattern, the 1 mm dots, having the highest frost coverage at approximately 90%. This means the smaller pattern led to a smaller overall frost surface coverage.

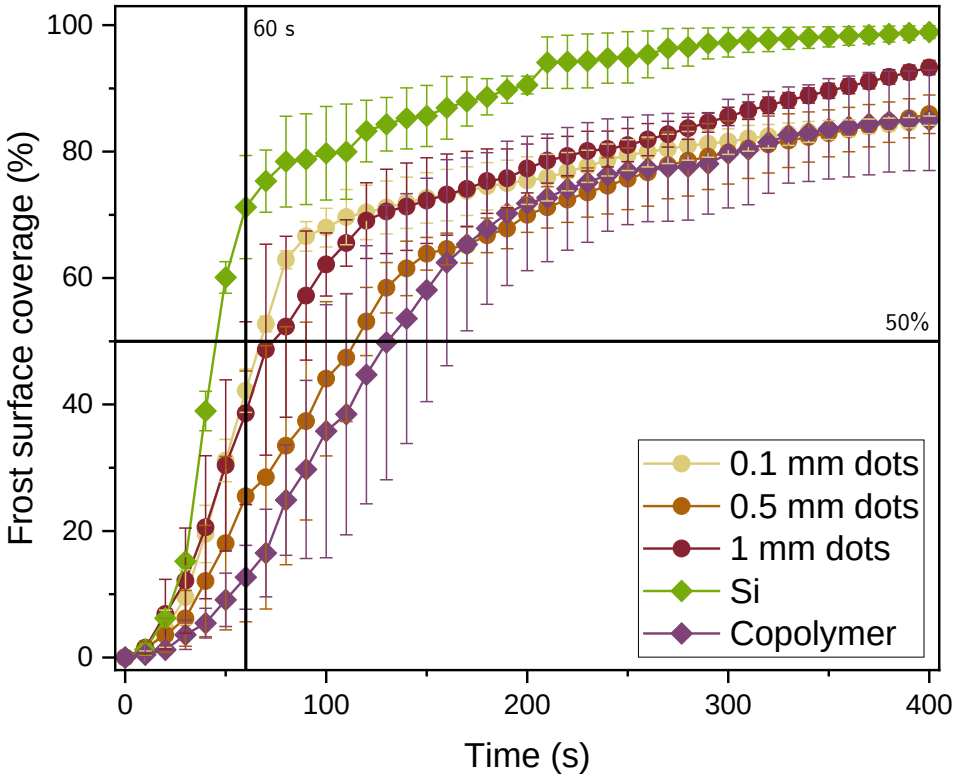

Figure 28: Frost propagation on the patterned biphilic samples and unpatterned copolymer and silicon.

6.2.3 Comparison between the two different surface types

The average of all the patterned hydrophobic and biphilic samples was calculated and compared with uncoated silicon and unpatterned copolymer surfaces.

In Figure 29 the evidence shows that all the coated samples delay and inhibit the frost propagation across their surfaces. They delay the frost propagation a lot longer compared to uncoated silicon. The hydrophobic patterned surfaces lead to an overall lower ice surface coverage. The biphilic patterned surface had a higher frost propagation compared to the patterned hydrophobic and copolymer surfaces. At the end of the experiment, the patterned biphilic surface performed similarly to the unpatterned copolymer surface. The patterned hydrophobic surface led to an overall reduced ice surface coverage.

After one minute, the uncoated silicon surface had the highest frost surface coverage, while the unpatterned copolymer surface had the lowest frost surface coverage. The patterned samples all had a frost surface coverage of below 50%. The copolymer reached a 50% frost surface coverage after roughly 130 seconds while the hydrophobic patterned surface reached the 50% coverage mark after only 110 seconds and the biphilic patterned surface reached the 50% mark in 80 seconds.

At the end of the experiment, the average frost cover for the silicon surface is close to 100% while the average frost cover for the copolymer surface is around 85%. The biphilic patterned surfaces had an 87% frost cover on average, while the hydrophobic patterned surface had only a roughly 77% surface coverage.

On average, the hydrophobic patterned surfaces had a larger frost propagation delay than the biphilic patterned surfaces. More fine waterdrops seemed to condense on the hydrophilic parts of the biphilic pattern. The hydrophilic base was plain silicon. Using a hydrophilic hydrogel as a base layer which might absorb some of the condensed water could lead to a reduced frost propagation. The patterned surfaces outperformed the uncoated silicon surface. The unpatterned copolymer surface had a slower frost propagation at the beginning of the experiments, but at the end, the frost coverage of the hydrophobic patterned surfaces was lower than the one of the unpatterned copolymers.

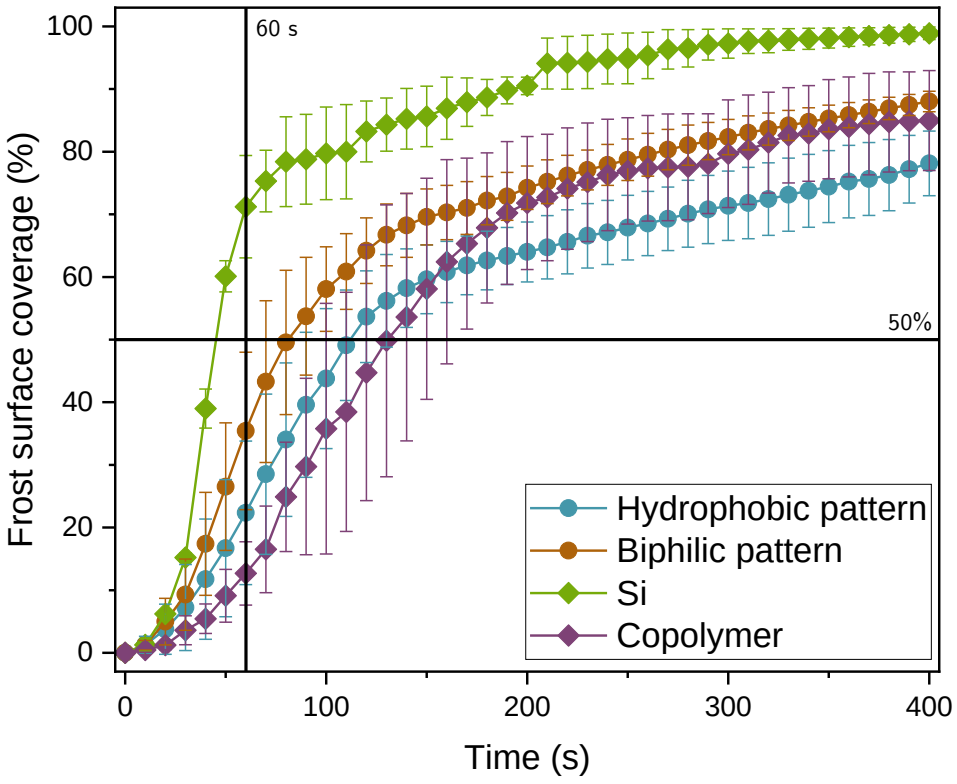

Figure 29: Comparison of the frost propagation on patterned hydrophobic and biphilic samples and unpatterned copolymer and silicon.

6.3 Summary

To sum up, it can be said that the patterned surface led to longer average freezing delays and slower frost propagation across their surfaces than the uncoated silicon surface.

The longest average freezing delay out of all the patterned samples was measured with the patterned biphilic surfaces. The smallest pattern with the 0.1 mm dots had the largest average freezing delay out of all the investigated patterned surfaces. With decreasing temperatures, the patterned samples had a larger average freezing delay than the uncoated silicon and even the unpatterned copolymer. On average, the biphilic patterned samples had a larger freezing delay than the hydrophobic patterned samples. Only at higher temperatures of -15°C, do the waterdrops on the unpatterned copolymer surface stay liquid longer than on the patterned surfaces. This means that the anti-icing effects of the copolymer are still effective, even if the entire surface is covered with it. The surface coverage does seem to affect the freezing delay, with the smaller patterns and lower surface coverage having higher average freezing delays than the other patterns most of

the time. The smallest patterns, both for the biphilic patterned surfaces and the hydrophobic patterned surface, had the largest average freezing delay.

The patterned hydrophobic surfaces had the slowest frost propagation and ice surface coverage. The biphilic patterned surfaces had a faster frost propagation at the beginning of the experiments, but at the end, the frost coverage of the biphilic patterned surfaces and the unpatterned copolymer were similar. This means the same delay in frost propagation and a similar prohibition of frost coverage is attained even when the samples are only partially covered with a copolymer. This indicates, that not the entire surface needs to be covered in an anti-icing copolymer for it to behave icephobic. The biphilic patterned samples had a faster frost propagation across their surfaces compared to the hydrophobic patterned surfaces.

It is of interest to note that the biphilic patterned surfaces had a higher freezing delay but a faster frost propagation. The anti-icing behaviour of this pattern type depends on how the water is placed on the surface and how it disperses. The hydrophobic patterns lead to slower frost propagation across the surfaces. Using a hydrogel instead of plain silicon could lead to slower frost propagation. The 5 µl waterdrops on the biphilic patterned surfaces tended to stay liquid the longest during the ice nucleation experiments.

7 Conclusion

To sum up, the hydrophobic patterned surfaces performed better in the ice nucleation tests, while the biphilic patterned surfaces performed better in the frost propagation tests.

The uniformly-coated copolymer surfaces were used as a reference to see if the surface coverage of the copolymer and the patterning affected the icing behaviour. It can be said that the patterned surfaces do delay the ice nucleation and frost propagation across the surfaces to some extent.

Not the entire surface needs to be covered in anti-icing copolymers to achieve similar effects. For frost nucleation, even a 13% surface coverage with icephobic copolymers leads to similar or better results than a uniformly covered surface. This means similar or better results can be achieved if the surfaces are textured and only parts of them are covered with icephobic copolymers.

The frost propagation across the surfaces is much more influenced by the type of the surface than the pattern size. The hydrophobic surfaces led to a slower frost propagation, while the biphilic surfaces had a faster frost propagation. The size of the pattern or the surface coverage by the dots seemed to have a very small influence on the frost propagation speed.

The coatings are easy to produce and reproduce. The patterning can be repeated or adjusted without difficulty.

It can be summed up, that the patterned samples showed anti-icing characteristics and not the entire surface needs to be covered in anti-icing polymers to achieve this effect.

8 Outlook

The ice nucleation tests were done at ambient humidity, which was on average approximately 30%. These tests can be repeated at very low ambient humidity and at high ambient humidity to measure the anti-icing effect of the surfaces in different conditions. These ice nucleation tests in different conditions were planned but could not be performed because of technical problems with the equipment in the lab during the experimental phase of this thesis.

With these measurements, more details about the behaviour of the patterned surfaces in different environments could be investigated. The average ice nucleation delay is expected to be a lot shorter in higher humidity and to be a lot longer in lower humidity.

All patterns had the same surface coatings with a combined thickness of 150 nm for the hydrophobic patterned samples and 300 nm thickness of the gradient copolymer dots for the biphilic patterned samples. The thicknesses of the coatings could be adjusted and increased for additional testing. A copolymer coating with a 50nm thick base layer of V4D4, a 150 nm thick copolymer and a 300 nm thick top coating of PFDA might exhibit even more anti-icing characteristics than the copolymer with only a 150 nm thick PFDA top coating.

8.1 Future steps

All the measurements of the patterned samples were done on surfaces that had circles in a grid pattern deposited with iCVD on them. Changing the pattern could influence the anti-icing behaviour. The circles in a grid pattern were chosen because the pattern is easily reproducible and the circles are isotropic. The behaviour of the waterdrops on the patterned dots is independent of direction. The pattern of the circles in a grid layout is not isotropic.

The experiments could be repeated with different patterns to inquire if other patterns lead to different icing behaviours. Straight copolymer lines or groves could lead to a directional depending icing manner. Water placed on these surfaces might move from the hydrophobic parts to the hydrophilic parts and it could be led to run off the surface that

way. Other structures like rectangles, starburst patterns, and hexagons with varying distances between them can also divert the water on the surface.

Completely isotropic patterns, like the ones achieved with $CuCl_2$, could also be tested. The varying sizes of the dots and the different distances between them would form a unique surface. The icing behaviour of water on them would be completely directionally independent.

The samples used were completely flat. Surfaces that are not entirely even would also affect how the water behaves. Similar to the beetle shell, a concave or convex surface would divert the water across it. Real-life applications for anti-icing surfaces are not only needed for completely horizontal surfaces. These types of substrates would be much more difficult to create and experiment with.

The surface types investigated were hydrophobic copolymer dots on a hydrophilic silicon base and hydrophobic dots on a hydrophobic base. Another approach would be to create hydrophilic spots on a hydrophobic base to see how this would affect the ice nucleation and frost propagation. These types of surfaces with hydrophilic structures on a hydrophobic base would be similar to the desert beetle shell. Attempts were made to create such surfaces, but they could not be deposited without being easily destroyed as soon as they came in contact with water. The decision was made to only test the samples with hydrophobic dots on either hydrophobic or hydrophilic base layers.

Other tests that were not conducted but could be of interest in the future are the ice adhesion test, where the forces required to remove ice frozen on the surface are measured. Supercooled droplet impact tests where the behaviour of supercooled water that is dropped onto cooled substrates is observed, could also be performed. Anti-icing surfaces can also lead to freezing point depression, which can be investigated. [10]

9 Bibliography

[1] K. Golovin, S. P. R. Kobaku, D. H. Lee, E. T. DiLoreto, J. M. Mabry and A. Tuteja, "Designing durable icephobic surfaces," *Science Advances,* 11 March 2016.

[2] X. Huang, N. Tepylo, V. Pommier-Budinger, M. Budinger, E. Bonaccurso, P. Villedieu and L. Bennani, "A survey of icephobic coatings and their potential use in a hybrid coating/active ice protection system for aerospace applications," *Progress in Aerospace Sciences,* pp. 74-97, February 2019.

[3] B. Jackson, "3D Printing Industry," 07 January 2019. [Online]. Available: https://3dprintingindustry.com/news/the-best-way-of-collecting-water-in-the-desert-3d-printed-beetles-cacti-or-grass-146523/. [Accessed 13 February 2024].

[4] B. Mohammadian, R. K. Annavarapu, A. Raiyan, S. K. Nemani, S. Kim, M. Wang and H. Sojoudi, "Delayed Frost Growth on Nanoporous Microstructured Surfaces Utilizing Jumping and Sweeping Condensates," *Langmuir,* p. 6635–6650, 16 May 2020.

[5] S. A. Khan, M. A. Atieh and M. Koç, "Micro-Nano Scale Surface Coating for Nucleate Boiling Heat Transfer: A Critical Review," *Energies,* 16 November 2018.

[6] X. Huang, M. Sun, X. Shi, J. Shao, M. Jin, W. Liu, R. Zhang and S. Huang, "Chemical vapor deposition of transparent superhydrophobic anti-Icing coatings with tailored polymer nanoarray architecture," *Chemical Engineering Journal,* 15 February 2023.

[7] K. K. Gleason, CVD Polymers: Fabrication of Organic Surfaces and Devices, Weinheim: Wiley-VCH, 2015.

[8] A. Coclite, "annacoclite.com," 2016. [Online]. Available: https://www.annacoclite.com/initiated-chemical-vapor-deposition-1. [Accessed 13 February 2024].

[9] Y. Cho, M. Lee, S. Park, Y. Kim, E. Lee and S. G. Im, "A Versatile Surface Modification Method via Vapor-phase Deposited Functional Polymer Films for Biomedical Device Applications," *Biotechnology and Bioprocess Engineering,* p. 165–178, 01 April 2021.

[10] M. Grizen and M. K. Tiwari, "Icephobic Surfaces: Features and Challenges," in *Ice Adhesion: Mechanism, Measurement, and Mitigation*, Weinheim, Wiley-VCH, 2020, p. 417–466.

[11] I. Roisman and C. Tropea, "Wetting and icing of surfaces," *Current Opinion in Colloid & Interface Science,* June 2021.

[12] Y. Liu, Y. Wu, S. Liu and F. Zhou, "Material Strategies for Ice Accretion Prevention and Easy Removal," *ACS Materials Letters,* pp. 246-262, 2022.

[13] M. Nosonovsky and V. Hejazi, "Why superhydrophobic surfaces are not always icephobic," *ACS Nano,* p. 8488–8491, 25 September 2012.

[14] Z. Zehui, C. Huawei, L. Xiaolin, W. Zelinlan, Z. Yantong and Z. Yuping, "The development of electric heating coating with temperature controlling capability for anti-icing/de-icing," *Cold Regions Science and Technology,* 19 January 2021.

[15] K. K. Varanasi, T. Deng, D. J. Smith, M. Hsu and N. Bhate, "Frost formation and ice adhesion on superhydrophobic surfaces," *Applied Physics Letters,* 2010.

[16] J. B. Boreyko and P. C. Collier, "Delayed Frost Growth on Jumping-Drop Superhydrophobic Surfaces," *ACS Nano,* p. 1618–1627, 3 January 2013.

[17] A. J. Meuler, D. Smith, K. K. Varanasi, J. M. Mabry, G. H. McKinley and R. E. Cohen, "Relationships between Water Wettability and Ice Adhesion," *ACS Applied Materials & Interfaces,* p. 3100–3110, 15 October 2010.

[18] S. Schröder, O. Polonskyi, T. Strunskus and F. Faupel, "Nanoscale gradient copolymer films via single-step deposition from the vapor phase," *Materials Today ,* pp. 35-42, 2020.

[19] G. Hernández Rodríguez, M. Fratschko, L. Stendardo, C. Antonini, R. Resel and A. M. Coclite, "Icephobic Gradient Polymer Coatings Deposited via iCVD: A Novel Approach for Icing Control and Mitigation," *ACS Appl. Mater. Interfaces,* p. 11901–11913, 24 February 2024.

[20] Y. Yoo, J. B. You, W. Choi and S. G. Im, "A stacked polymer film for robust superhydrophobic fabrics," *Polymer Chemistry,* February 2013.

[21] P. Kwong, C. A. Flowers and M. Gupta, "Directed Deposition of Functional Polymers onto Porous Substrates Using Metal Salt Inhibitors," *Langmuir,* p. 10634–10641, 12 August 2011.

[22] DuPont, "DuPont: Polyimide Films," DuPont de Nemours, Inc., [Online]. Available: https://www.dupont.com/electronics-industrial/polyimide-films.html#headingacc1. [Accessed 14 February 2024].

[23] E. Alizadeh-Birjandi, A. Alshehri and H. P. Kavehpour, "Condensation on Surfaces With Biphilic Topography: Experiment and Modeling," *Frontiers Mechanical Engineering,* 25 June 2019.

[24] H. Jo, H. S. Park and M. H. Kim, "Single bubble dynamics on hydrophobic–hydrophilic mixed surfaces," *International Journal of Heat and Mass Transfer,* pp. 554-565, 11 November 2015.

[25] A. Al-Sharafi, B. S. Yilbas and H. Ali, "A Water Droplet Pinning and Heat Transfer Characteristics on an Inclined Hydrophobic Surface," *Scientific Reports,* 15 February 2018.

[26] J. E. Castillo, Y. Huang, Z. Pan and J. A. Weibel, "Quantifying the Pathways of Latent Heat Dissipation during Droplet Freezing on Cooled Substrates," *International Journal of Heat and Mass Transfer,* January 2021.

[27] Z. Zhu, X. Zhang, Y. Zhao, X. Huang and C. Yang, "Freezing characteristics of deposited water droplets on hydrophilic and hydrophobic cold surfaces," *International Journal of Thermal Sciences,* January 2022.

[28] A. D. Sommers, C. W. Gebhart and C. J. L. Hermes, "The role of surface wettability on natural convection frosting: Frost growth data and a new correlation for hydrophilic and hydrophobic surfaces," *International Journal of Heat and Mass Transfer,* pp. 78-88, July 2018.

[29] M. R. Haque, S. R. Das and A. R. Betz, "Experimental investigation of condensation and freezing phenomena on hydrophilic and hydrophobic graphene coating," *Applied Thermal Engineering,* September 2019.